Chapter 1

Introduction, theoretical descriptions of spontaneous combustion phenomena and aims of this thesis

1.1. Introduction

The spontaneous combustion of materials has been observed for over 1000 years. Pliny (1st century AD, book XVIII) reported the occurrence of spontaneous ignition in freshly stacked grass. It was not, however, until beginning of the 19th century that spontaneous combustion phenomenology was examined from a scientific perspective by researchers such as van't Hoff in 1844.

The issue of spontaneous combustion has commonly been associated with coal where it is a safety, industrial and environmental problem (Carras and Young, 1994). This problem is widespread in many industries and Bowes (1984) has provided a comprehensive discussion of self-heating for many materials including coal and coal products and for a large range of cellulosic materials including hay, wood fibre and cotton.

A description of self-heating is complex, as the phenomenon is caused by the difference between the rate of heat loss and the rate of heat generation within a reactive substance. The rate of heat generation depends on the exothermic chemical process, which in most cases is not well understood. Correspondingly, the heat loss rate depends upon physical parameters such as conductivity and convectional surface loss, which while fundamentally well understood, may not be accurately known for the material in question.

It should be noted that throughout this thesis, the term 'self-heating is used to define the general occurrence where material retains a portion of the reaction heat within the material itself and heats a few degrees above ambient temperature. The term 'thermal ignition' will used to describe the specific form of self-heating whereby the heat retention leads to a rapid and accelerative increase in the internal

temperature of the body. This definition originates from the fundamental physical and theoretical concepts of spontaneous combustion phenomenon. The definition arises from the thermal behaviour of the material and as such, it is not a requirement that active smouldering or flames develop; although in many cases this is the case. This definition has been used by Bowes (1984, page 23, 187, 463) who also describes this behaviour as a 'thermal explosion of the first kind'. This definition is important for reactive inorganic materials, such as calcium hypochlorite, where the substance may exhibit accelerative thermal behaviour and decompose to produce temperatures of several hundred degrees but not smoulder or produce flames in isolation. Hence, with this type reactive material, it is only when this material is near combustible substances, such as when packed within plastic drums, that there exist the potential for active smouldering and flames. This is an important distinction for the studies discussed in the latter chapters of this thesis.

This thesis focuses on two materials that display self-heating behaviour; bagasse, the fibrous residue that remains from sugar cane processing and calcium hypochlorite, a substance commonly used as a biocide. These two materials, while chemically and physically quite dissimilar, exhibit related problems for each respective industry.

Bagasse is produced in many millions of tonnes every year by Australian sugar processing mills. The material, which is approximately 50% by mass water, is similar to chopped grass. It is used as a fuel by the sugar processing mills and large quantities of bagasse are stockpiled onsite. Bagasse is also stored between subsequent crushing seasons and used as the initial fuel source at the commencement of the following season. Typical industrial stockpiles generally range in size from 200 to 100000 tonnes and once formed, self-heat to temperatures of approximately 65°C (Dixon, 1988). While the majority of stockpiles remain stable at this temperature, for reasons unknown, some stockpiles continue to self-heat until the bagasse ignites. It is this self-heating problem of bagasse that is the focus of the first two chapters of this thesis.

The second material discussed in this thesis is calcium hypochlorite. In common with bagasse, the material has for many years been associated with conflagrations as a result of thermal ignition. This substance is transported in many thousands of tonnes about the globe and has been associated with numerous conflagrations aboard cargo vessels. The latter chapters of this thesis examine the thermal ignition phenomenology of this substance.

1.2. Theoretical models for Self-heating

1.2.1. The Semenov steady state model

The Semenov formulation (1928) stands as the first attempt to quantify the problem of thermal ignition and has traditionally been used to introduce the theoretical concepts of criticality, the energy balance between heat release and heat loss rate as well as the existence (or otherwise) of stable and unstable steady states. The Semenov model focuses on the heat balance between the non-linear (with respect to temperature) heat release rate of a self-heating substance and the simultaneous linear heat loss rate to the surrounding environment. The non-linearity arises from the exponential rate dependence of the reaction kinetics, which for the generalised case, is given by:

$$\dot{q}_G = VQf(c)e^{\frac{-E}{RT}} \qquad [1.1]$$

where $\dot{q}_G$ is the rate of heat generation, V and Q are the volume and the molar heat of reaction. The rate function f(c) is generally assigned a simple relationship defined as $f(c) = Zc_0^n$, where c_0^n is the initial reactant concentration of reaction order n and Z, is the Arrhenius pre-exponential constant. The original Semenov analysis defines zero order reaction kinetics with respect to reactant concentration, however, this is not a restriction of this generalised form. The exponential term $e^{-E/RT}$ is the Arrhenius temperature dependence term with E being the apparent activation energy and R the ideal gas constant and T is temperature.

The Semenov model also assumes Newtonian cooling where the heat transferred to the surroundings is given by:

$$\dot{q}_L = S\chi(T - T_a) \qquad [1.2]$$

where $\dot{q}_L$ is the rate of heat loss, S is the surface area and χ is the heat transfer coefficient. A spatially uniform temperature (T) is defined within the material with heat loss occurring as a temperature discontinuity at the boundary surface while T_a is defined as a uniform and constant ambient temperature. This heat loss condition, while useful as a first approximation method, especially for materials with a high conductivity or stirred fluids is not reflective of the temperature distribution within common reactive solids since these have lower conductivities. A further and necessary assumption of this model, which is common to all thermal ignition models, is that the chemistry is sufficiently temperature sensitive (activation energy sufficiently large) that kinetic acceleration leading to thermal ignition can exist.

The two processes described by equations 1.1 and 1.2 give rise to two of the central concepts of thermal ignition theory; the heat balance between the heat release rate and the heat loss rate and criticality. The essential elements of this concept can be qualitatively introduced by way of heat generation and heat loss loci such as those shown in figure 1.2.1.

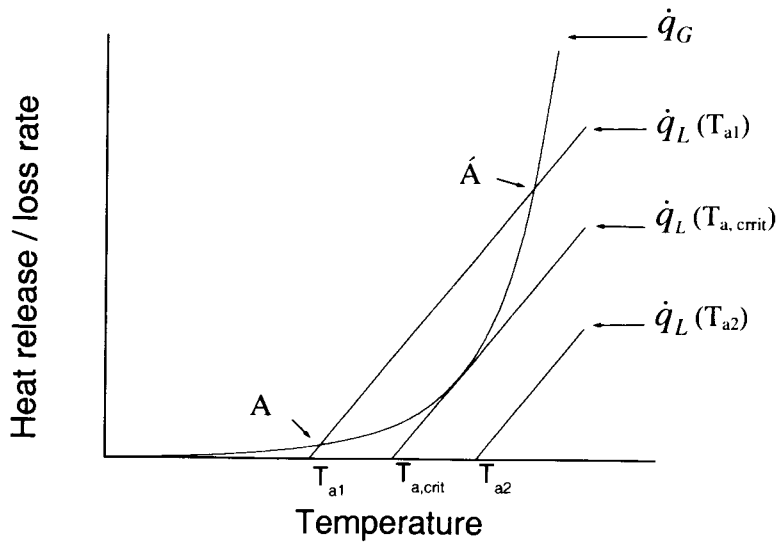

Figure 1.2.1: Heat generation and heat loss loci with respect to temperature for sub-critical, supercritical and critical conditions.

Figure 1.2.1 shows the highly convex nature of the exponential Arrhenius heat release curve for the temperature range that is usually encountered by most thermal ignition and self-heating problems. Also shown are three heat loss curves for a body of fixed given size and maintained at ambient temperature T_{a1}, $T_{a,critical}$ and T_{a2}. The heat loss loci T_{a1}, shows the existence of two solutions (A, Á) representing balanced conditions for equations [1.1] and [1.2]. The lower temperature balance point (A) occurs close to ambient temperature (T_{a1}) and is recognised as a stable balance point. The stability of this point can be shown by considering the energy balance at temperatures slightly greater than and less than that of the balance point. At slightly higher temperatures, the heat loss rate exceeds the heat release rate and so the temperature of the body tends to return to the balance condition. Conversely, at temperatures slightly less than the balance point, the heat release rate exceeds the heat loss rate and the body self-heats to the balance condition. Notice that the temperature of the body at the balance point is greater than Ta_1. This temperature rise represents the sub-critical self-heating condition and manifests itself as a temperature rise

of a few degrees within the substance. This self-heating may not directly lead to active smouldering and flames, but may cause significant damage as a result of stock and produce deterioration.

The second solution displayed for loci T_{a1} (Á) is considered an unstable condition since a small perturbation from this critical temperature will result in either, cooling to the lower temperature balance point, or heating to thermal ignition. Notice that at temperatures above this point, the heat release rate exceeds the heat loss rate while at reduced temperatures, the converse relationship exists. Due to this condition, this point is also defined as the 'critical stacking temperature' (CST) and represents the maximum temperature of the actual self-heating substance from which a body can be formed without thermal ignition occurring. When the body is formed from self-heating material at a temperature below the CST, the body cools to a temperature close to the stable balance point, A; conversely, if the self-heating material is at a temperature above the CST, then the body self-heats to thermal ignition. It should be noted that the upper temperature balance point has not been shown in figure 1.2.1 since it occurs at several thousand degrees Kelvin and as such, is outside the temperature range of normal self-heating phenomenon.

When the ambient temperature experienced by a body is increased from T_{a1} to $T_{a,critical}$, then the stable and unstable balance points move towards each other and eventually merge at the point of tangency. This point represents the limit of stable behaviour of the body and once this temperature is exceeded, the body will self-heat to ignition. While the heat loss loci $T_{a,critical}$ shows the existence of only one balance point, loci T_{a2} shows the disappearance of stable balance points resulting in the body self-heating to ignition at all temperatures. Super-criticality for the current assumptions and conditions can therefore, be defined as simply the condition where a balance between the heat release rate and heat loss rate of a body cannot be achieved. The result of supercritical behaviour is generally more experimentally obvious than that of sub-critical behaviour and is defined as 'thermal ignition' (defined in section 1.1). This phenomenon usually leads to active smouldering and the occurrence of flames, however, it should be noted that active smouldering and flames are not required for thermal ignition to occur. It should be noted that throughout

this thesis, the term Critical Ignition Temperature (CIT) will be used to identify the above critical temperature $T_{a,critical}$ and distinguish this theoretical ignition temperature from experimentally approximated critical temperatures. The experimentally determined critical temperature will be defined later in this thesis.

An analogous interpretation to that used to describe the temperature dependence of criticality can also be used to examine the dependence of criticality with respect to the radii or the size of a self-heating body. Figure 1.2.2 conceptually illustrates the existence of balance points for equations 1.1 and 1.2, but this time for increasing radii bodies maintained at a fixed temperature.

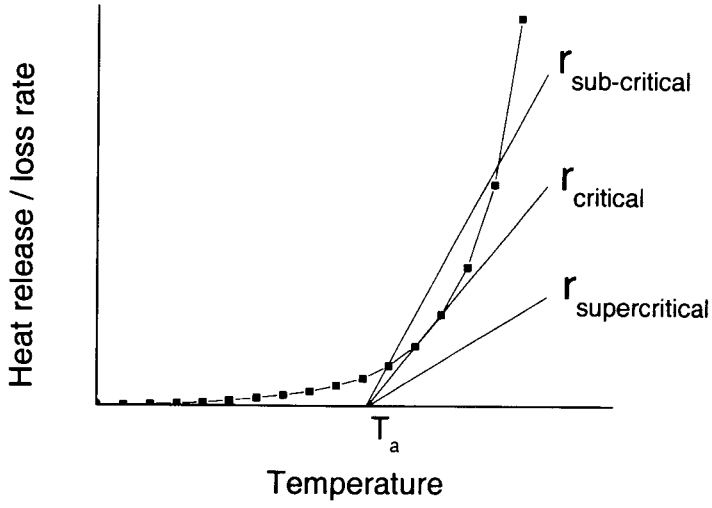

Figure 1.2.2: Heat generation and heat loss loci with respect to radius for sub-critical, supercritical and critical conditions.

Figure 1.2.2 shows a similar heat generation loci to that shown in figure 1.2.1 as well as three heat loss loci. The heat loss loci are shown as lines with successively reduced heat loss rates, representing three bodies with successively larger radii. Heat loss loci $r_{sub\text{-}critical}$ again shows the existence of two balance points that eventually merge as the radius of the body becomes larger. These balance points again merge at the point at the tangency and corresponds to the largest body that is capable of displaying stable behaviour for a given value of ambient temperature. Loci $r_{supercritical}$ shows the disappearance of balance

points for radii greater than $r_{critical}$ resulting in the same supercritical consequences as discussed for figure 1.2.1.

The two equations that describe the conservation of energy and the kinetic rate law are:

$$C_v \rho V \frac{dT}{dt} = VQf(c_0^n)e^{\frac{-E}{RT}} - S\chi(T - Ta) \qquad [1.3]$$

and:

$$\frac{dc}{dt} = -f(c_0^n)e^{\frac{-E}{RT}} \qquad [1.4]$$

where C_v and ρ are the heat capacity at constant volume and density respectively. Other parameters have been defined previously (see equations 1.1 and 1.2) and t is time.

The above equations assume that the temperature within the body is spatially uniform and that the reaction kinetics is described by a single reaction of simple integral order. In addition to the above criteria, the heat generation rate of the reaction must also be sufficiently large and the reaction kinetics sufficiently temperature sensitive to produce accelerative thermal behaviour. Considering firstly the case where Q is small and the heat loss term is of a realistic magnitude, then it can be seen that heat loss rate will exceed the heat release rate and no critical behaviour will be displayed. In the second case where the activation energy is small, the heat release rate becomes very insensitive to temperature rise and provides insufficient accelerative thermal behaviour to support criticality. Hence, while self-heating may occur in this second case, critical behaviour is not displayed.

The right hand side of equation 1.3 is the difference between the heat release rate (1.1) and the heat loss rate (1.2) and represents the amount of heat retained by the self-heating material. Equation 1.4 describes the rate of fuel consumption over time and while not included in the original Semenov formulation, this equation enhances the usefulness of the model since reactant consumption is included. While these two equations are not analytically soluble, the critical conditions can be identified using bifurcation theory and

as such, this heat balance has been found useful for describing the self-heating behaviour of high conductivity material and as a demonstrative tool.

1.2.2. The Frank-Kamenetskii Theory of Criticality

In contrast to the Semenov model (1928), the Frank-Kamenetskii (1969) model uses Fouriers's Law of heat conduction in conjunction with the assumption that no thermal resistance occurs at the surface boundary of the body to account for self-heating phenomena. This purely conductive approach inevitably implies that thermal resistance occurs entirely within the body itself and hence, predefines the existence of a temperature gradient within the body. The Frank-Kamenetskii model is a good approximation of many scientific and industrial self-heating problems and as such, is most commonly used for the interpretation of experimental thermal ignition data. In its original form, however, the Frank-Kamenetskii model, like the Semenov model, is considered an extreme version of real self-heating phenomena with the true condition existing somewhere between these two cases (Thomas, 1958).

The equation that describes the steady state heat balance of Frank-Kamenetskii theory is:

$$\kappa\nabla^2\theta T + Qf(c_0)e^{\frac{-E}{RT}} = 0 \qquad [1.5]$$

with the boundary condition $T = T_0$ on the wall(s) of the body. ∇^2 is the Laplacian, κ is the thermal conductivity with the other parameters are defined previously (see equations 1.1 and 1.2). As is the case with the classical Semenov model, the original Frank-Kamenetskii model assumes that unlimited reactants are available. A full discussion of further formulations of this model that include reactant consumption can be found in the monograph of Bowes (1984). While not soluble analytically, Frank-Kamenetskii approximated the Arrhenius temperature dependence term for one-dimensional infinite slab geometry with the assumption that E is large. A similar approximation was also shown by Chambre (1952) to be analytically soluble for infinite cylinder geometry. By recasting temperature T in terms of ambient temperature T_0 and a temperature difference $T- T_0$, Frank-Kamenetskii (1969) approximated the temperature dependence by reasssigning T in the form:

$$T = T_0[1 + (T - T_0)/T_0] \qquad [1.6]$$

and since $(T - T_0)$ is very small compared to T_0 near criticality, the exponent of the Arrhenius temperature dependence can be approximated by:

$$\frac{E}{RT} = \frac{E}{RT_0[1 + (T - T_0)/T_0]} \approx \frac{E}{RT_0}(1 - \frac{(T - T_0)}{T_0}) = \frac{E}{RT_0} - \frac{E}{RT_0^2}(T - T_0) \qquad [1.7]$$

By introducing a dimensionless variable which is proportional to the temperature excess of the self-heating material where:

$$\theta = \frac{E}{RT_a^2}(T - T_a) \qquad [1.8]$$

then equation 1.7 can be presented as:

$$= \frac{E}{RT_0} - \frac{E}{RT_0^2}(T - T_0) \equiv \frac{E}{RT_0} - \theta \qquad [1.9]$$

Hence, equation 1.5 can now be expressed in a dimensionless form as:

$$-\nabla^2\theta = \delta \exp\theta \qquad [1.10]$$

where δ is the Frank-Kamenetskii number defined as:

$$\delta = (Q/\kappa)r^2(E/RT_0^2)A'c_0 \exp(-E/RT_0) \qquad [1.11]$$

and $z = x/r$.

where z is a dimensionless distance and is a function of the radius of a cylinder or sphere or the half-thickness of a slab and x is the distance coordinate measured at the origin.

For infinite slab geometry:

$$\nabla^2\theta = \frac{d^2\theta}{dz^2} \qquad [1.12]$$

And for infinite cylinder geometry:

$$\nabla^2\theta = \frac{d^2\theta}{dz^2} + \frac{1}{z}\frac{d\theta}{dz} \qquad [1.13]$$

Hence, assuming symmetric heating, the centre maximum condition is defined by:

$$\frac{d\delta}{dz} = 0 \text{ at } z = 0 \qquad [1.14]$$

with the boundary condition:

$$-\frac{d\delta}{dz} = \alpha\theta \qquad [1.15]$$

at the boundary surface where z = ± 1. In this case δ is the dimensionless temperature rise at the surface of the body and α is the Biot number, which is defined as:

$$\alpha = \frac{\chi r}{\kappa} \qquad [1.16]$$

The Biot number is a dimensionless measure of the ratio of the thermal resistance within a body to thermal resistance at the surface of the body and has important implications with respect to the suitability of the classical Frank-Kamenetskii or Semenov model to an experimental situation. This aspect will be further discussed later in this chapter.

For the above boundary condition, solutions to equation 1.10 exist for a limited range of δ and never exceed a critical value defined as δ_{crit}. In the case where δ exceeds δ_{crit}, no steady state solutions exist and the body will self-heat to thermal ignition. Bowes (1984) has tabulated both δ_{crit} and θ_{crit} values at infinite Biot number and for a range of geometries with the geometries that will be discussed in this thesis being listed in Table 1.2.1.

Table 1.2.1 $\delta_{crit,(\infty)}$ and $\theta_{crit,(\infty)}$ values for geometries discussed in this thesis.

Geometry	$\theta_{crit,(\infty)}$	$\delta_{crit,(\infty)}$
Infinite plane slab, thickness 2r	1.119	0.878
Infinite cylinder, radius r	1.386	2.00
Short cylinder (Equicylinder) radius r, height 2r	1.778	2.76

Equation 1.10 can be rearranged into a logarithmic form that enables the theoretical interpretation of experimental thermal ignition data, the form of which is defined by:

$$\ln\left[\frac{\delta_{crit}T_{0,crit}^2}{r^2}\right] = M - \frac{N}{T_{0,crit}} \qquad [1.17]$$

where:

$$M = \ln\left[\frac{QEA'c_0^z}{R\kappa}\right] \quad \text{and} \quad N = \frac{E}{R} \qquad [1.18]$$

Hence, a plot of $\ln[\delta_{crit}T_{a,crit}^2/r^2]$ against $1/T_{a,crit}$ displays a straight line with slope –E/R and intercept $\ln[QEA'c_0^z/R\kappa]$ for a single reaction mechanism with Arrhenius temperature dependence.

The above relationship is central to conventional thermal ignition measurements, where the temperature delineating the supercritical and sub-critical behaviour of the substance is experimentally determined over a range of sample sizes of known geometry. Classical critical ambient temperature measurements involve packing the sample to a known density in a stainless steel gauze basket while 'hot' (at a temperature a few degrees below the test temperature). The basket is then quickly placed within a temperature controlled forced convection oven. A small temperature sensor is also generally located at the geometric centre of the body to monitor the temperature history of the body over the measurement. A series of experiments are repeated at different temperatures until both sub-critical and supercritical behaviour is observed over a narrow temperature range. The measurements are completed for a range of basket sizes and the CAT is assigned for each basket size from the mean of the closest sub-critical and supercritical oven temperatures. These data are interpreted using equation 1.17, which enables fundamental chemical parameters to be determined while also allowing the CAT's of larger bodies to be predicted using an extrapolation of the experimental data.

While the 'classical' CAT test involves the 'hot assembly' of the basket, in cases such as where the test material releases toxic gases or where there is the possibility of explosion, it is not possible to assemble the test container using preheated sample. In these cases the sample is assembled cold and the entire sample and container placed into the preheated oven. The test sample is entirely warmed within the test container. The interpretation of 'cold assembly' CAT data, therefore, requires that the reactant consumption, which occurs during the warm up period, must be either small and hence, neglected or accounted for in the interpretation. For materials where E/R is large, the kinetics is sufficiently temperature sensitive that reactant consumption can be neglected during the initial warm up period (Bowes. 1984, page 187). Clearly, this is an important aspect since the results of 'cold assembled' CAT tests may give misleading results where reactant consumption is appreciable during the warm up period. Hence, a careful understanding of the experimental requirements of this test is required if accurate meaningful results are to be obtained and the results interpreted correctly. It should be noted that the CAT

measurements involving hydrated calcium hypochlorite were completed using a cold assembly method. The hot assembly method was used at an early stage in this study, however, it was not continued due to safety concern relating to the large concentrations of chlorine gas that were produced during the assembly of the basket. Given that the E/R value measured in the latter chapters of this thesis was of the order of 5 x 10^3 $kJmol^{-1}$ for hydrated calcium hypochlorite, the activation energy of this material is in the sufficiently high range to neglect reactant consumption.

1.3. Factors affecting the theories of self-heating

1.3.1. Finite Biot number and implications.

The magnitude of the calculated Biot number is a particularly important indicator for assessing the suitability of the surface heat transfer assumptions of the Semenov and Frank-Kamenetskii models for a particular experimental situation. Theoretically, the Biot number can range between zero and infinity, however, experimentally, its value generally lies between these two extreme values. Thomas (1957, 1959) originally revealed that both the Semenov ($\alpha \rightarrow 0$) and the Frank-Kamenetskii ($\alpha \rightarrow \infty$) models are limiting cases of a more general formulation that describes the heat transfer boundary condition at the edge of a body. Thomas (1957, 1959) identified that significant uncertainties could arise when δ_{crit} values at infinite Biot number were used to interpret experimental thermal ignition data in situations where the magnitude of the Biot number for the body approached the lower limit of α. Generally it is found that δ_{crit} is sensitive to Biot number of a body over the range from about $0 < \alpha < 30$.

To account for condition where a body exhibits a finite Biot number, Thomas (1959) and Barzykin et al (1966) have used semi-empirical functions to correct δ_{crit} ($\alpha = \infty$) over the range where it is sensitive to the Biot number of the body. Bowes (1984) discusses this aspect in detail and describes an extended formulation that includes further corrections for reactant consumption and finite activation energy (Boddington et al, 1983). The general formulation consists of three correction factors that are of the form:

$$\psi_{1(\alpha)} = \frac{\alpha}{2}\left(\sqrt{\alpha^2+4}-\alpha\right)\exp\left(\frac{\sqrt{\alpha^2+4}-\alpha-2}{\alpha}\right) \qquad [1.19]$$

$$\psi_{2(B)} = 1+\frac{2.4}{B^{2/3}} \qquad [1.20]$$

$$\psi_{3(u)} = 1+u \qquad [1.21]$$

where $\psi_{1(\alpha)}$ is the correction for finite Biot number, $\psi_{2(B)}$ is the correction for diminishing reactant concentration and $\psi_{3(u)}$ is the correction for finite activation energy. The parameter B in equation 1.20 governs the effects of reactant consumption and is defined as:

$$B = \frac{EQc_0}{RT_0^2\rho C_v} \qquad [1.22]$$

This parameter can be interpreted as the adiabatic temperature rise of the body.

The correction for finite activation energy and hence, the reduced acceleration of the reaction kinetics with temperature, is accounted by the equation 1.21 where u is defined as:

$$u = \frac{RT_0}{E} \qquad [1.23]$$

Bowes (1984) combines these three correction parameters in the form:

$$\delta_{crit,(\alpha,B,\varepsilon)} = \delta_{crit,(\infty)} \cdot \psi_{1(\alpha)} \cdot \psi_{2(B)} \cdot \psi_{3(u)} \qquad [1.24]$$

enabling increased accuracy in the determination of fundamental chemical parameters from experimental data where the assumptions of the Frank-Kamenetski model do not explicitly hold.

1.3.2. Industrial implications of self-heating materials with finite Biot number

The sensitivity of δ_{crit} to α for materials under conditions where the calculated is $\alpha < 30$, means that the CAT of a body is also a function of the surface heat loss condition. In practical terms, this translates into CAT's that are sensitive to the experimental convection (fan forced or natural) conditions. This sensitivity has significant safety ramifications for industry and safety regulation agencies since the current test procedure that is used to determine the maximum 'safe' storage and transport temperature of self-heating materials, the United States self-accelerating decomposition temperature test or SADT test (United Nations, New York and Geneva, 1995), does not address the potential influence of the convection conditions of the test environment upon the safe storage temperature reported. Hence, for materials where the calculated Biot number is $0 < \alpha < 30$, the SADT, has the potential of measuring a 'safe' storage temperature that is several degrees higher than the 'safe' storage temperature that would otherwise be measured under natural convectional conditions. This important aspect is discussed in detail later in this thesis.

1.3.3. The role of interactive self-heating in estimating CAT's of large assemblies of self-heating bodies.

If a large number of individually self-heating bodies or thermons (Gray, 2000, Boddington et al,1982, Boddington et al,1984) are placed within a heat bath of finite heat capacity, such as a fully enveloping and tightly fitting box that itself does not touch the individual bodies, then the CAT of a single isolated body

will not necessarily be representative of the CAT of the entire assembly. The origin of this difference lies in the additional thermal resistance that is now placed between the thermons and the exterior air environment. This barrier may result in the accumulation of heat within the enclosed air environment resulting in an increase in the local temperature experienced by each thermon. Hence, the boundary conditions at the surface of each thermon will now be time dependent with respect to both ambient temperature and convection conditions with the latter now being a function of the thermal gradients within the airspace. This is a problem of high importance to storage and transport industries as well as transport regulation agencies since this is precisely the condition that exists when drums of self-heating material are tightly packed within an enclosed truck or commercial transport container. While seemingly an obvious problem, this area has received little scientific investigation. Boddington et al (1982) has examined this problem with respect to the storage and transport of propellants, however, it is only recently that this problem has been examined from the perspective of transport within standard shipping containers (Gray, 2000). In the Gray analysis, the overall heat balance of an assembly as well as the influence of the surface heat loss condition of the individual bodies, was examined for the 'well-stirred' case, that is, the simple case where no temperature gradients existed between the 'n' self-heating bodies. The heat balance for each individual body was defined by:

$$c_v \rho v \frac{dT_i}{dt} - vQZ \exp(-E/RT_i) - \chi s(T - T_i) \qquad [1.25]$$

$$i = 1,\ldots,n \qquad T_i(0) = T_i^0$$

and that of the surrounding container when filled with n bodies (drums/pails/kegs etc) by:

$$c_v' \rho' v' \frac{dT}{dt} \chi s \sum_{n-1}^{n} (T_i - T) - \psi S(T - T_0) \qquad [1.26]$$

where T_i is the spatially constant temperature of each individual body and v is the volume of each individual body. It was assumed that reactant concentration remained constant. The parameters c_v', ρ' and

v' are the heat capacity at constant volume, the density and the volume of the air inside the surrounding container when filled with n bodies while ψ is the heat transfer coefficient at the surrounding container wall. Since the walls of the container surrounding the individual bodies are thin, the surface heat transfer of the surrounding container arises mainly from convectional processes and is almost independent of the conductivity of the surface material type. A similar condition applies at the surface of each thermon and since two convectional exchanges occur at the container wall, it is possible to approximate the heat transfer coefficient of the wall as being equal to twice the heat transfer coefficient of the individual thermon.

It is worth noting the requirement that surrounding container volume v' must be larger than nv and that co-operative self-heating diminishes as v' increases relative to nv (providing sufficient air space exists between each thermon). Hence, for the above assumption and in the extreme case where v' is very large compared to nv, the thermons will behave as independent entities. Additionally, for the extreme case of a large assembly consisting of a very large number of small thermons, the behaviour of the assembly will tend to approximate that of a single body with a reduced bulk density.

The formulations of Gray (2000, 2002) have shown that a wide range of behaviour is theoretically possible depending upon the initial conditions and nature of the individual bodies. These calculations also showed that the spatial position of the maximum temperature may not necessarily be at the geometric centre, but may exist anywhere between the geometric centre of the container and the outermost layer of thermons. Irrespective of the point of ignition, for the current assumptions, the calculations invariably suggested that a significantly lower CAT would be expected for the assembly. Clearly, for the industrial conditions where thermal gradients may exist between each thermon, further reductions in CAT, compared to the more conservative well stirred approach, would be expected The industrial ramifications of the calculations of Gray (2000) will be further discussed later in this thesis.

1.3.4. Parallel reactions

Independent parallel reactions of 'zero order' have been investigated in a general form by Abramov, Vaganov and Samoilenko (1975, 1977, 1978) and have been further discussed by Bowes (1984). The Abramov et al formulation introduces an effective heat release function that combines the activation energy, heat release rate and and the Arrhenius frequency factor for each individual reaction into a temperature dependent function describing the overall kinetics. The formulation is expressed by a conventional Arrhenius equation defined as:

$$\frac{dq}{dt} = \sum Q_i A_i e^{\frac{-E_i}{RT}} = Q^* A^* e^{\frac{-E^*}{RT}} \qquad [1.27]$$

In this equation Q* is the effective heat of reaction, A* is the effective Arrhenius pre-exponential factor and E* is the effective activation energy.

While the Abramov et al treatment provided a comprehensive account of parallel heating systems, in many cases, especially where two reactions having relatively different activation energies exist and the area of interest is not over the transition area between the two reaction regimes, then each reaction can be considered to operate independently over a limited temperature range. This is shown graphically in figure 1.2.4.

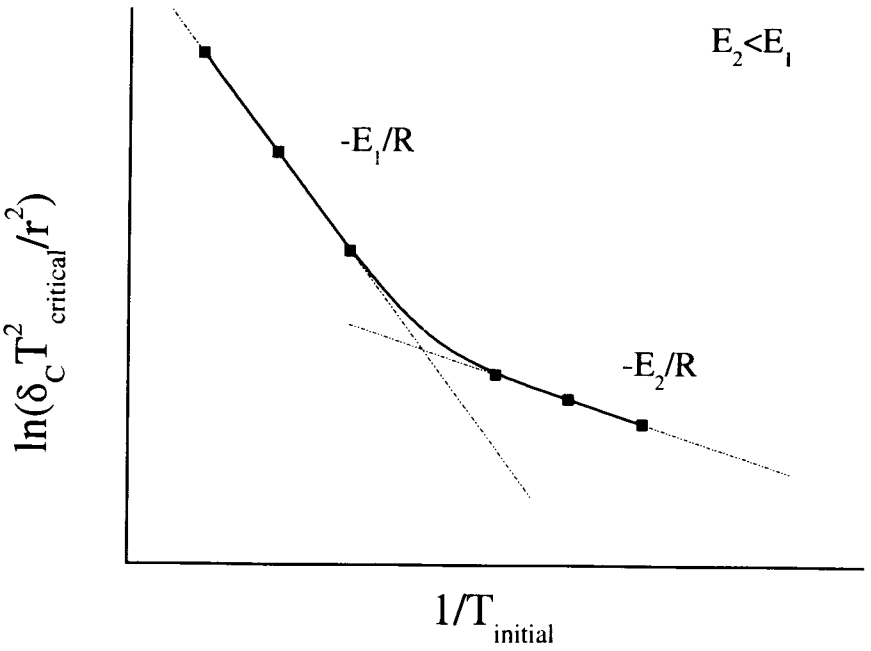

Figure 1.2.4: Traditional Frank-Kamenetskii plot representing a self-heating system comprising of two parallel reaction mechanisms.

This figure represents a system where two exothermic reactions with significantly different activation energies exist. In this current figure, each mechanism can be seen to play a greater part in the reaction kinetics over a limited temperature range, with the low activation energy reaction playing a greater part in the reaction kinetics at lower temperatures. The non-linearity of the current data clearly shows that experimental CAT's estimates for large bodies that are derived from long extrapolations of the higher temperature reaction data would significantly overestimate the true critical ignition temperature. This aspect has serious implications for standard industrial 'tests' methods (Jones, 1999; Chen, 1998) where for expediency, a single measurement is performed or measurements are performed over a limited temperature range. For such cases, the conditions of the tests may not correctly identify the non-linear kinetic behaviour of the material resulting in possibly dangerous consequences. Generally, industrial tests such as those suggested above and empirical tests such as the Mackey test (1895, 1896) are useful for assessing the hazard of a substance under the specific test conditions only, and as such, inferences regarding more general spontaneous combustions behaviour or hazards could be significantly flawed.

Clearly, to confidently estimate the critical ignition temperature of large bodies, measurements need to be completed over a wide range of temperatures and on a sufficiently large scale so that the full self-heating kinetics is elucidated.

1.3.5. The presence of water.

The presence of water within a spontaneously combustible material may significantly modify the chemical and physical properties of that material. In the case where water does not directly take place in the self-heating chemistry, the presence of water generally modifies the bulk physical properties of the material such as the bulk heat capacity, density and conductivity. Furthermore, evaporative processes may increase the heat loss condition in the overall heat balance, potentially resulting in the inhibition or delaying of the onset of thermal ignition. Experimentally, this aspect may be seen as no more than an increase in the time to ignition in the case of the supercritical behaviour, or an increase in the time to reach the maximum temperature rise, in the case of the sub-critical behaviour. This feature is generally displayed in orthodox laboratory criticality measurements as a reduction in the rate of temperature rise as a body approaches a characteristic temperature where the water phase is lost by evaporation. This feature has been observed in orthodox criticality measurements of cellulosic materials such as bagasse (the extracted residue from sugar cane refining which may contain up to 60% water on a wet basis), cotton and hay, where an inflection is observed in the heating rate as the sample temperature approaches 100°C (Sisson 1991).

While the physical impact of water upon a self-heating material may be clearly identified and readily interpreted using traditional formulations, the chemical influences may be subtle, difficult to interpret and significantly more influential upon the overall self-heating behaviour. In the case of commercial grade hydrated calcium hypochlorite, the chemical influence of water has been significantly misinterpreted by the industry resulting in the underestimating of the self-heating hazard of this substance (Gray and Halliburton, 2000).

In cases where water plays an active role in the self-heating chemistry, either as a solvent or as a reactant, the self-heating material may be influenced by a 'wet reaction'. In this case, the presence of water plays a role in both the heat loss and heat generation terms of the heat balance. Many cellulosic materials are known to exhibit this type of chemistry in addition to the 'dry' reaction chemistry that exists at increased temperatures. The quantification of this type of chemistry requires special considerations from an experimental perspective since orthodox criticality tests at normal laboratory sizes will be incapable of examining the low temperature reactivity due to the loss of sample moisture. For these types of materials, alternative experimental methods such as isothermal calorimetry techniques are required to measure the self-heating phenomenology.

Recently Macaskill, Sexton and Gray (1998) have modelled the self-heating of stored bagasse using formulations that consider the evaporation, condensation and diffusion of water throughout the stockpile as well as the wet and dry oxidation chemistry. The model was originally proposed by Sisson et al.(1992) and consists of a four variable system of PDE's, where the variables are liquid and vapour phase water, temperature and oxygen. The Macaskill, Sexton and Gray (1998) model, uses the formulations of Sisson et al, (1991) as well as formulations describing the density of the stockpile as a function of the liquid water concentration.

1.4. Aims of this thesis

It is clear from the preceding discussion that the behaviour of self-heating materials can be very complex and that much of this complexity can be captured by appropriate mathematical formulations. However, in order to apply the more general models to real materials of commercial and industrial importance, such as bagasse and calcium hypochlorite, an understanding of the chemical behaviour of these materials is required. Of particular interest are the rates of chemical reaction and associated heat release. Once the chemical and thermodynamic behaviour has been elucidated so that it can be incorporated into the models for self-heating, it is also important to ascertain how well the models perform in describing the behaviour of these self heating materials in realistic simulations. These two issues form the major thrust of this

thesis. However in order to satisfy these two general aims a number of more specifics objectives were required. These are described below.

1.4.1. Specific aims of the Bagasse section

For bagasse details of the nature of the chemical reactions and the role of water are poorly understood. Consequently the aims of the work presented in this thesis on bagasse were:

1) To establish the relationship between the oxidation rate and heat release rate of bagasse.
2) To establish the effect of water upon the oxidation rate and heat release rate of bagasse.
3) To quantify the effect of temperature upon the oxidation rate of bagasse.
4) To quantify the self heating behaviour of large bagasse stockpiles and to compare their behaviour with the predictions of the model developed by Macaskill, Sexton and Gray (1998, 2001).
5) To quantify the effect of density upon the self-heating behaviour of bagasse stockpiles with geometries suitable to enable accurate comparisons with the predictions of Macaskill, Sexton and Gray (1998, 2001).

1.4.2. Specific aims of the Calcium hypochlorite section

The aims of the work presented in this thesis on calcium hypochlorite were:

1) To quantify the apparent activation energy and Arrhenius pre-exponential kinetic constant for the decomposition of this material.
2) To quantify the critical ambient temperature of commercially transported quantities of calcium hypochlorite.
3) To establish the thermal ignition behaviour of this material when individual drums of this material are packed into a confined space.

This thesis describes two quite different materials, each with its own characteristic chemical, industrial and safety issues. The work is presented as two independent studies with chapters two and three detailing the work on bagasse while chapters four, five, six and seven describe the work on calcium hypochlorite. The results of each investigation are preceded by an introduction, which describes the state of knowledge of self heating of each material prior to the work carried out for this thesis. The important findings from the current work are summarised at the end of each Chapter as well as in the Conclusion.

Chapter 2

Laboratory measurements of the self-heating phenomenology of Bagasse.

2.1. Self-heating of Bagasse

The safe storage of bagasse over extended periods, has been an ongoing problem for the Sugar Industry. During the past 16 years there have been 10 confirmed outbreaks of spontaneous combustion within commercial bagasse storage stockpiles in Queensland, Australia. One documented occurrence at Pioneer Mill, located near Townsville, burned for several months (Dixon, 1997) and another recent occurrence at Invicta Mill, also located near Townsville, destroyed a valuable stockpile of bagasse bales that were designated to be used for electricity co-generation (Dixon, 2000). The loss of this valuable fuel from spontaneous combustion has significant economic, environmental and safety implications for the sugar industry. As more mills utilise the bagasse for co-generation, the economic implications will become increasingly significant.

Published investigations into the self-heating properties of cellulosic materials have most commonly centred upon the low temperature heating chemistry of wet hay. Following nearly a century of investigation, conflict remains not only as to the magnitude of the heat release, but also, to its origin (Dixon 1988). The relative contribution of biological and chemical heating to the total energy balance has remained a topic of debate, with little research undertaken into the elucidation of the contribution of the latter, at low temperatures (Ashbolt 1986). The heating chemistry of bagasse has received far less investigation than that for hay and the literature reveals a noticeable lack of published data.

For hay, research into the spontaneous combustion has been undertaken using a range of small-scale experimental techniques and large-scale field tests (Truninger, 1929; Hoffmann, 1940; Musselman, 1935). Other measurements have indicated (Rothbaulm, 1963), that the heating chemistry is very sensitive to material water content and relative humidity. While this early research attributed the origin of the thermal rise within hay stockpiles to biological activity, no investigation was undertaken to determine the numbers of active microbial species present within the active media. Later, larger scale

experiments (Dixon 1988) on chemically treated bagasse stockpiles have revealed, that the low temperature heating of this material could be attributed almost entirely to chemical heating, with the microbial component contributing insignificantly to the heat balance. Heat release calculations (Gray 1984) using measured active thermophilic microbe populations for bagasse (Ashbolt 1986) concluded, that an initial temperature rise of 2°C per day could be sustained during the initial heating of a bagasse stockpile. Experience, however, has demonstrated that during the construction of full-sized bagasse stockpiles, heating rates of up to 20°C per day are achievable (Ashbolt 1986), well in excess of the calculated values.

Early research work (Gray et al, 1984) concentrated on the combustion of dry bagasse, which is initiated by a high temperature oxidation process. These results gave useful information regarding bagasse as a fuel, but were unable to describe the low temperature heating chemistry of wet bagasse. Following further experimental work carried out by Sisson (1991) on wet cotton and bagasse, it was concluded that an unknown, low temperature, water mediated oxidation reaction was responsible for the initial heat production leading to the spontaneous combustion within stockpiles of cellulosic materials. The high temperature heat producing reaction of bagasse, as measured in laboratory critical ambient temperature measurements (CAT), has an activation energy in the order of 110kJ/mol. At temperatures below ~100°C, this reaction is negligibly slow. Correspondingly, the prediction of the heating behaviour of commercial sized stockpiles of wet bagasse require a model that accounts for the dry reaction, as well as the wet reaction. The spatial effects of evaporation, condensation and moisture movement within the stockpile, will also need to be considered.

Preliminary experimental calorimetric investigations (Gray and Carras, 1995) have revealed a wide variety of bagasse heating behaviour. This limited study detailed that at least two distinctive heating processes take place when dry air accesses moist bagasse. The first reaction was characterised by a rapid initial decline in reaction rate, followed by a long, very slow reaction decay. The second reaction process required the presence of both free water and oxygen and was identified to be the wet reaction discussed by Gray and co-workers earlier. This limited investigation elucidated a number of complex results concerning the oxidation of bagasse. It was concluded that a more detailed and thorough

investigation was required before the low temperature wet heating chemistry of bagasse was completely understood.

This chapter reports laboratory oxidation and calorimetric measurements on bagasse that are aimed towards identifying the nature of the heat release rate of the 'wet' oxidation chemistry of bagasse. The calorimetry measurements involved the utilisation of an isothermal calorimeter that is located within the Commonwealth Scientific and Industrial Research Organisation (CSIRO), Division of Energy Technology, North Ryde, Sydney. Australia.

2.2. Bagasse properties

The tissues of all woods and sugar cane contain the same major components with the proportions of each component varying according to the species or variety. Slight variation may be found at different parts of the plant and under different climatic conditions (Dixon 1988). Table 2.1 lists the constituents of Australian bagasse.

Table 2.1: Typical analysis of Australian bagasse (Dixon 1988).

Constituent	%
Bagasse Constituents (wet basis)	
Moisture	44 – 53
Brix	1 - 2
Ash	1 - 5
Fibre Constituents (dabf)*	
Cellulose	45 – 55
Hemicellulose	20 – 30
Lignin	15 - 26
Proximate Analysis of Fibre (daf)**	
Hydrogen	6.0
Oxygen	44.7
Carbon	49.0
Sulphur	0.03
Nitrogen	0.27

* Dry, ash and brix free.

** Dry, ash free.

2.3. Origin of the bagasse test samples

The bagasse test samples were obtained from Sugar Research Institute (SRI), Mackay, Queensland. Four samples were obtained from different seasons. One sample was obtained during the 1996 crushing season, two samples were obtained from the 1997 season and one sample was obtained from the 1998 crushing season. The samples were removed from the final bagasse processing conveyer belt, following the final crushing and sugar extraction processes. The hot, wet samples were sealed in plastic bags and transported to the Sugar Research Institute (SRI), Mackay, Queensland. There they were cooled and then transported overnight to CSIRO laboratories, North Ryde, New South Wales, where they were stored at -18°C until use. It should be noted that the major component of the work described in this chapter was completed using bagasse sample from the 1997 season.

2.4. Bagasse moisture content measurement

The moisture content of each bagasse test sample was determined gravimetrically upon arrival and prior to each experimental measurement. Test sub-samples were dried to constant mass at 105°C

within an atmosphere of dry nitrogen. The results of this elevated temperature method were also compared to sub-samples that were vacuum dried at 25°C. Negligible differences in moisture concentration were measured between each of the two drying methods and hence, for reasons of efficiency, the thermal drying technique was adopted as the standard method. The bagasse samples supplied from the SRI consistently contained a typical moisture content of 100% (dry basis).

2.5. Oxidation rate measurements

The oxidation rate was measured by exposing ~ 0.2kg of bagasse to an accurately measured flow of air and then determining the decrease in oxygen flux across the sample, at constant temperature and pressure. Preconditioned air, as discussed later in this chapter, was passed through each sample reactor vessel at a measured and constant rate. The stream selected exhaust gas was analysed by an on-line automated gas chromatograph (GC). The GC measured oxygen, nitrogen, carbon dioxide and carbon monoxide using a thermal conductivity detector (TCD). Before entering the GC, the reactor exhaust gas stream was passed through a water trap, controlled at a temperature of 1°C. Flow rates were controlled using needle valve flow controllers and continuously monitored over the 10 minute period immediately before each GC measurement using a 'Top Track' flow meter (Sierra Instruments INC, model 822-1). The flow readings of the 'Top Track' flow meter were also checked on a daily basis using a 'bubble' flow meter with all flows corrected for humidity where appropriate. During some experiments, the exhaust gas was also passed through a magnesium perchlorate packed drying tube. Magnesium perchlorate was utilised due to its low affinity for the species under investigation. Figure 2.5.1 shows a schematic diagram of the apparatus.

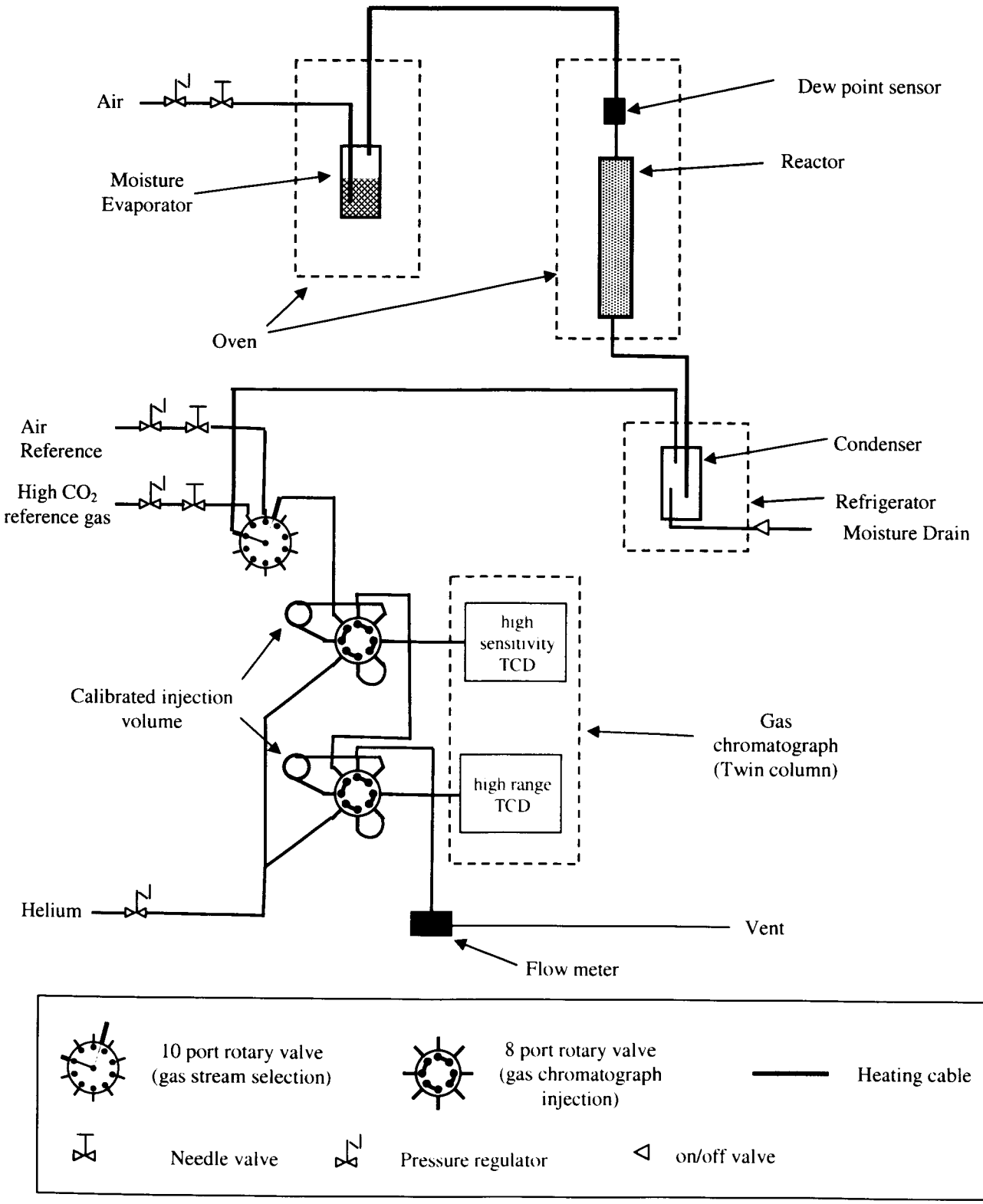

Figure 2.5.1: Schematic diagram of the Oxidation reaction system. Only one reactor circuit is shown.

The Hewlett Packard 5890 series GC used during reactor oxidation measurements was equipped with two separate and parallel GC columns (Altech 'CTR-II') and detectors. Helium (BOC UHP grade)

was used as a 'carrier' gas. The carrier gas was further conditioned prior to use by passing it through separate moisture (anhydrous potassium perchlorate) and oxygen (Alltech 'OXY-TRAP') scrubbing traps. The GC detectors were independently configured, one to a high concentration range setting (0.05 - 100%) and the other to a low concentration range setting (50 - 2000ppm). This configuration allowed, by way of two separate injections, a dynamic range from 50 ppm to 100% to be achieved. The above resolutions were possible for the permanent air gases, except for CO, which proved difficult to resolve below 1000ppm. On occasions, a non-dispersive infra-red (NDIR) CO analyser was used to measure CO concentrations in the gas stream. This instrument was, however, available only on a small number of occasions and the results should be considered as indicative only. Using the NDIR CO analyser, CO concentrations of up to 1000 ppm were measured during experiments at 50°C.

The apparatus was automated and could be operated unmanned for an indefinite period. While up to eight individual reactors could be run at any one time, it was found that six reactors was a manageable maximum.

The rate of oxygen consumption per unit mass for each material was calculated from the flow rate and the difference between the inlet and outlet oxygen concentrations. On the assumption that the nitrogen in the feed air was conserved, the rate of oxidation was calculated from the expression:

$$R_{(ox)} = [O_{2(in)} - O_{2(out)} (N_{2(in)} / N_{2(out)})]F/m \qquad [2.1]$$

Where $R_{(ox)}$ is the oxidation rate, expressed as moles of oxygen per gram of reactor charge per second, $O_{2(in)}$ and $N_{2(in)}$ are the oxygen and nitrogen inlet molar concentrations to the reactor. $O_{2(out)}$ and $N_{2(out)}$ are the outlet oxygen and nitrogen molar concentrations, F is the airflow through the reactor and m is the mass of the reactor charge.

In order to approximate a constant gaseous oxygen concentration across the reactor, a small oxygen deficit was maintained across the reactor. This meant that it was required to alter the airflow through the reactor occasionally during the course of the experiment. The oxygen deficit was typically limited

to ~ <3%. Experiments were carried out at a range of temperatures from 35 to 90°C and over a range of bagasse moisture contents. Experiments were run for periods of up to 10 weeks or until the oxidation rate stabilised.

The CO_2 flux was calculated from an expression similar to that used for the oxidation rate calculation.

The GC response to O_2, N_2 and CO_2 was periodically checked during the experiment by way of two methods. Firstly, a reference air supply (BOC instrument grade) was routinely passed through the instrument and analysed during each gas stream selection cycle enabling the drift of the TCD detector to be assessed. For a significant number of measurements, the air reference was supplemented with a second and higher CO_2 concentration (nominally 2.5%) reference gas so that two reference measurements were completed during each sample sequence. The second reference method involved directly comparing the response of the TCD to a standard calibration gas ('Scott Specialty Gases', SCOTTY® II 'MIX 218' and SCOTTY® II 'MIX 217'). This comparison was typically completed weekly and this was also used to standardize the references gases used for the online calibration.

To produce reactors that are filled with bagasse at uniform and relatively similar packing densities, each reactor vessel was packed using a standardised method. The process involved the loading and tamping (with constant pressure) of small quantities of bagasse progressively into the reactor. The loading and tamping process continued until the reactor was approximately 95 % full after which the reactor was sealed and leak tested. Leak free reactors were then placed within a preheated and temperature controlled fan forced oven.

Depending upon the GC timing cycle, gas analysis commenced from 2 to 8 hours after the beginning of the run. For the typical flow rates used in these experiments (~1 to 10cm^3/min), the time to effect one volume change (for a loaded reactor) was between ~ 30 and 110 minutes.

2.6. Calorimetry

2.6.1. Calorimeter Design

The heat of oxidation was measured directly using an isothermal calorimeter designed and constructed for oxidation measurements of dry coal (Nordon et al 1985). The calorimeter consists of two concentric brass cylinders that are approximately 150mm long and separated by a small air gap. The inner cylinder contains the sample charge (in a snug fitting removable insert to facilitate simple changing) while the exterior surface of the outer cylinder is maintained at constant temperature within a fan forced oven that has a temperature stability of better than ±0.1°C. During exothermic measurements, the heat generated by the reacting sample produces a small temperature gradient between the sample and the exterior surface of the calorimeter assembly. The maximum temperature gradient, however, exists across the air gap between the two brass cylinders and as such, it is this region that is used to measure the heat evolved from a reacting sample. To measure the small temperature gradient that develops across this air gap a thermopile, or large array of thermoelectric junctions, is located within the air gap.

Figure 2.6.1 shows a simplified version of the isothermal calorimeter.

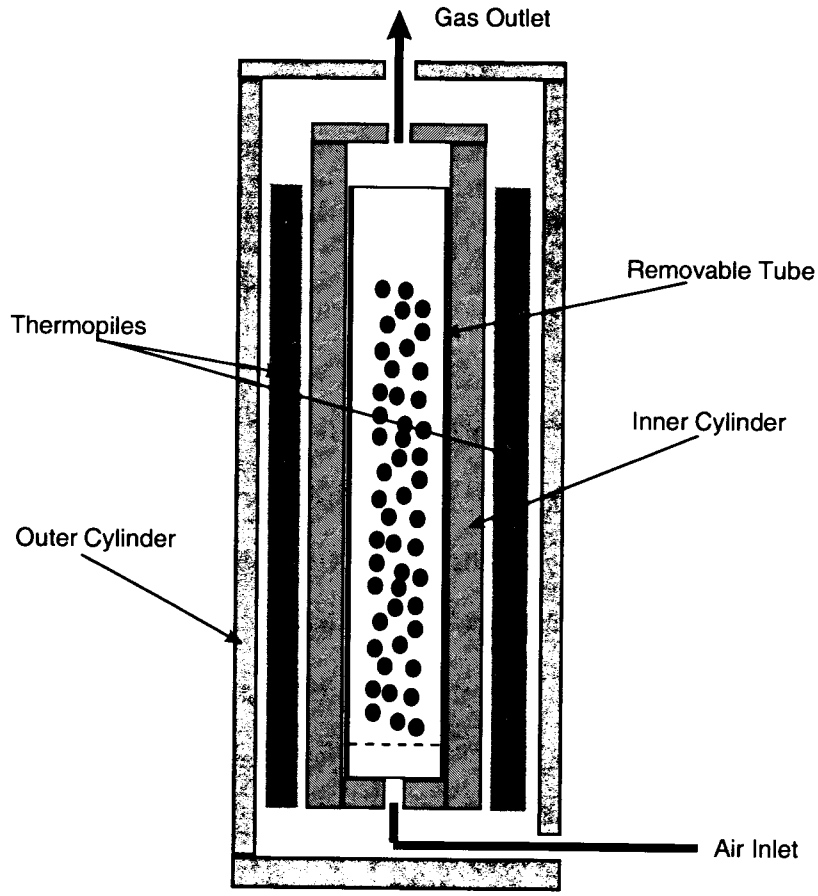

Figure 2.6.1: Simplified elevation and plan diagram of the isothermal calorimeter. The ancillary equipment is not shown. (This diagram was kindly provided by S.J. Day).

The thermopile assembly consists of 14 individual temperature sensitive elements equally spaced within the air space that forms the temperature-sensing region of the calorimeter. Each thermopile element is shaped in the form a wire helix and is constructed from 68 constantan/copper thermoelectric junctions. Each thermoelectric junction of the helix is electrically connected in series and arranged so that successive junctions are positioned on alternate (opposite) sides of the helix. When located within the air space that forms the temperature sensing region of the calorimeter, each helical element is insulated from the inner and outer brass cylinder by a thin 'Teflon' membrane (0.05 mm). The helix is also positioned so that the opposing thermoelectric junctions are located on each side the air space. A thin balsa wood spacer is inserted through the helix to provide structural strength and maintain contact between the thermoelectric junction and the Teflon covered inner and outer brass surfaces. By aligning the 952 thermoelectric junctions that comprise the entire thermopile in this way,

the thermal sensitivity of the thermopile is maximized producing a calorimeter thermal sensitivity of about ~ 10^{-6} W/g of sample charge.

To increase the overall thermal sensitivity of the measurements a combination of two identical calorimeter assemblies were used. Each calorimeter assembly was positioned within the oven so that both devices experienced identical thermal environments. Both calorimeter assemblies were filled with a common mass of bagasse using the method that was discussed in section 2.5. One calorimeter assembly, identified as the 'reference' calorimeter, was used to provide a measure of the thermal noise within the oven. The other calorimeter assembly, identified as the 'test' calorimeter, was used to provide a measure of both the thermal noise within the oven as well as the heat released by the exothermic bagasse reactions. Hence, by subtracting the thermal noise measured by the 'reference' calorimeter from the total heat release measured by the 'test' calorimeter, the thermal sensitivity of the measurements was significantly increased. It should be noted that the above subtraction assumes that the two samples of bagasse are identical in origin, mass, density and moisture concentration throughout the experiment.

Following the loading of the bagasse sample into each calorimeter assembly, nitrogen gas was initially passed through both the 'reference' and the 'test' calorimeters until a constant voltage was measured at the outputs of both calorimeter thermopiles. By initially flushing each calorimeter with an inert gas, the oxidation reactions of both bagasse samples were suppressed, enabling the thermal noise and thermal coupling between the two calorimeters to be measured. It should be noted that throughout all calorimetric measurements, the thermopiles of both calorimeters displayed a very large degree of thermal coupling once the calorimeters achieved thermal equilibrium. It is this high degree of coupling that enabled the accurate subtraction of thermal noise from the 'test' thermopile output. Once stable thermal behaviour was achieved by both the 'test' and 'reference' calorimeters, while being flushed with nitrogen, the gas supply to the test calorimeter was changed to air without change in flow rate. Following the gas change of the 'test' calorimeter to air, the electrical outputs of both calorimeters continued to be measured at hourly intervals with the electrical output of the 'test' calorimeter now being a measure of the heat released from bagasse oxidation.

Flow rates were measured using a 'bubble' flow meter, with flow readings corrected for humidity. Flow rates were accurately controlled using two identical mass flow controllers (Brooks model 0152E, range 0 – 3 standard cm^3/min). These were shown to be stable and drift free over long periods of time and hence, enabled the flows through each calorimeter to be accurately matched. Typical flow rates ranged from 0.4 to 3 cm^3 per min. The oxidation rate of the test sample was measured in a similar way to the reactor experiments. A Gow-Mac GC (Series 350) was used to monitor the O_2, N_2 and CO_2 concentrations in this case. The system is automated to allow unattended operation.

The heat generated from the bagasse, Q, in watts per g of bagasse, was calculated from the expression:

$$Q = SC/m \qquad [2.2]$$

where S is the thermopile output, m the mass of the sample and C the calibration factor specific to the sample calorimeter. The calorimeter apparatus was also equipped with a GC in a similar manner as to that outlined in section 2.5. This enabled oxidation rates to measured in concurrently with the heat of reaction.

Prior to the present series of measurements, the minimum calorimeter operating temperature was 55°C. To undertake the measurements below 55°C, modifications to the air circulation and temperature control systems were undertaken. These modifications enabled the lowering of the operating temperature to 30°C.

Early experimental measurements revealed some incompatibility between the bagasse oxidation products and the materials used in the construction of the sample vessel. The viton o-rings and gaskets sealing the sample vessel deteriorated during experiments and the brass inner sample vessel corroded. Following one early measurement, the sample vessel corroded in position and was completely destroyed in the extraction process. These problems were overcome through the fabrication of a very

thin 316- grade stainless steel sample cylinder and through the use of 'ethylene propylene diene' monomer (EPDM) rubber seals.

2.6.2. Calibration of the calorimeter thermopile

During the course of this investigation the thermal response of the thermopile was measured on two occasions (table 2). The results of these calibration tests deviated from previous calibration tests by less than the magnitude of the experimental uncertainty.

Table 2.2: Measured thermopile calibration factors.

Details of calibration	Calibration factor
Bainbridge 1985	0.00001638 Js^{-1}
Bainbridge 1988	0.00001638 Js^{-1}
Halliburton 1996	0.00001696 Js^{-1}
Halliburton 1997	0.00001642 Js^{-1}

2.7. Moisture control.

Preliminary calorimetric measurements (Gray and Carras, 1995) identified the need to control the test sample moisture content during oxidation measurements. It was found during the preliminary series of measurements, that the dry airstream flowing into the reaction vessel dried the test sample to a value where bagasse activity was significantly altered.

To undertake the present, more detailed, moisture dependent measurements, techniques were developed to precondition the moisture content of the sample inlet gas stream. Throughout all of the tests discussed in this report, maintaining constant sample moisture remained a difficult task due to the open, flow-through nature of the reaction vessel and long time periods required for each test to reach steady state.

A large range of methods were investigated to humidify the inlet gas stream. Eventually an oven/evaporator method was developed to pre-condition the gas stream. For bagasse test samples with moisture contents above the maximum moisture content value, that is, where free water is formed on the bagasse surface, a saturated air stream was passed into the reaction vessel. For tests below the maximum moisture regain value, an air stream pre-conditioned to the adsorption isotherm humidity value of the bagasse sample, was used. The above critical humidity value was determined gravimetrically using constant humidity salt solutions.

2.8. Detailed description of the gas supply and humidification apparatus

Either preconditioned nitrogen or air was passed through the test sample and reference sample at controlled and measured rates using the mass flow controller units described in section 2.6.1. Two different humidification methods were used to humidify the gas streams depending upon the required humidity. Identical methods were used for both the reference and the test gas streams during each individual measurement run with type of method selected being determined from the analysis of the initial moisture content of the bagasse sample. In the case where the bagasse contained free water, a saturated gas stream was used. To produce gas streams saturated with water, the gas leaving the flow controller was initially passed through a vessel (0.5L volume and defined here as the evaporation vessel) containing a quantity of distilled water (~0.25L). The evaporation vessel was contained within a separate oven which was thermally controlled to a temperature slightly greater than the air temperature within the calorimeter oven. The humidified feed gas exiting the evaporation vessel was then carried through heated stainless steel tubing (heated to 110°C) to a second oven that contained the calorimeter assemblies. The stainless steel tubing entered through the side of the calorimeter through a small tubular opening located approximately half a metre above the oven floor. After entering the oven, the gas stream was passed through additional stainless steel tubing which terminated at a second stainless steel vessel (0.5L). This second vessel was positioned in the lower portion of the calorimeter oven and was used as a 'catch pot' to collect water condensate. It should be noted that after the stainless steel tubing entered the calorimeter oven, the tubing was aligned in a continuously downward direction enabling the condensate to flow into the catch pot. The catch pot and evaporator vessels incorporated the facility to monitor and replenish/remove water with minimal disturbance to the

reaction airflow. After the catch pot, the now saturated gas stream passed through additional stainless steel tubing (~ 0.5m) before entering the calorimeter housing. This additional tubing was aligned vertically for approximately half its total length to facilitate the 'back' collection of the remaining condensate into the catch pot. During initial measurements, a second catch pot was also connected in-line between the first catch pot and the calorimeter assembly. It was found, however, that no condensate was collected in this second vessel and its use was not continued.

For the moisture content measurements where the humidity of the gas stream was less than the saturation concentration, the gas stream was passed through up to four additional vessels containing constant humidity salt solutions. It should be noted that the air stream that entered the first of these four additional vessels was firstly pre-humidified to within a few of degrees Celsius of the dew point of the saturated salt solution using the evaporation/condensation method described above. Hence, the saturated salt solutions were essentially used to 'fine tune' the final humidity. The composition of the constant humidity salt solutions was chosen on the basis of the final humidity required to maintain constant moisture mass within the bagasse sample. It should be noted that the method discussed in the section was found to be more effective in producing stable humidity conditions within each gas stream over long periods of time than by using the saturated salt solutions alone. It was observed that when only saturated salt solutions were used to humidify the dry gas metered from the mass flow controllers, it became more difficult to achieve constant humidity, with the saturated salt solutions generally drying out quite quickly. A 'chilled mirror', dew point meter was used to measure the dew point of the reactor inlet gas stream prior to measurements.

2.9 Preparation of Test Samples

2.9.1 Reactor sample preparation

The test samples were manually separated into individual bagasse fibres and lightly packed into a clean reactor. The packing process was carefully undertaken to produce a uniform packing density of 0.35g/cm^3 dry mass. The temperature of the bagasse at the completion of the loading process was

typically 5 –10°C. During the sample loading process, a sub-sample of bagasse was removed and the moisture content determined using the standard method.

For moisture measurements below the nominal 100% (dry basis), the bagasse sample was placed into a vessel constructed to allow efficient purging of the bagasse with dry nitrogen gas. During the purging process, the sample mass was periodically measured and the purging terminated when the predetermined moisture content was reached. At all times during the drying process the test sample remained at or below 10°C. The reduced moisture sample was chilled and then packed into the reaction vessel in the standard manner with a sub-sample of bagasse taken for accurate moisture content determination. This method minimised sample preconditioning from heating and/or oxidation from the drying process.

During the development of the packing procedure for the reactors, a study was also undertaken to examine the effect of shredding the bagasse into a smaller fibre size. The shredding operation of the bagasse was undertaken at SRI and both shredded and non-shredded, but otherwise identical, samples were examined. The final maximum fibre length of the shredded bagasse, as supplied, was approximately 5 to 6mm as compared to a fibre length of approximately 25 to 35 mm for the unprocessed bagasse sample. Comparative oxidation tests, undertaken at 50°C, showed a similar behaviour for both the processed and unprocessed samples.

2.9.2 Calorimeter sample Preparation

The sample preparation for calorimeter measurements was identical to that used for reactor preparation except that just prior to the packing of the reaction cell, the larger fibre particles (above 5mm) were removed from the sample. This was done to facilitate the even packing of the smaller calorimeter reaction cell.

During initial bagasse calorimetry measurements, tests comparing the reactivity of the pith and the fibre components of the bagasse as well as the effect of shredding the bagasse into smaller fibre, were undertaken. Initially, shredding was attempted using a domestic blender and a "kitchen whiz". Both

appliances were found to be ineffective due to the toughness of the fibre with the long processing times unavoidably resulting in significant heating of the sample. An industrial ball mill located at SRI was finally used to efficiently grind the test sample to a maximum fibre length of 5 to 6 mm. Test results between the pith and fibre components as well as processed and non-processed sample showed similar behaviour for the otherwise identical bagasse sample. For measurements discussed in this chapter unprocessed samples were used.

2.10. Moisture Sorption of dried bagasse samples

At the commencement of this current study, literature revealed a paucity of moisture sorption data relating to the equilibrium moisture concentration of bagasse at humidities from 10 to 100%. Hence, to determine the approximate moisture concentration of the inlet gas stream required to maintain a constant bagasse moisture concentration during calorimeter or reactor measurements, the constant humidity moisture sorption content of bagasse was measured at a number of temperatures. The moisture of bagasse was measured gravimetrically using a dessicator/constant humidity method. The bagasse sample was oven dried within an atmosphere of dry nitrogen. Sub-samples of known mass were then placed into weighing jars and exposed to separate atmospheres of nitrogen that were maintained at constant humidity. The mass of each sub-sample was regularly measured until a constant mass was achieved. Separate measurements were completed over the humidity range from 7 to 98% and at temperatures from 3 to 80°C. The constant humidity atmosphere for each measurement was maintained by way of a saturated salt solution with accurately known equilibrium humidity (Wexler and Seinfeld, 1991; Greenspan, 1977). While this method is experimentally simple, it is slow, with some measurements requiring several weeks to reach constant moisture content. A further disadvantage of this method was that at the time of weighing, the bagasse sub-samples were withdrawn from the equilibrium environment and hence, for a short time, the bagasse sample experienced conditions other than those that were maintained within the desiccator. While not a problem for ambient temperature measurements, at increased and reduced temperatures, the bagasse samples cooled or heated to room temperature within the weighing jars, which were sealed at that time. To minimise the influence of the environmental change that the samples experienced during weighing process, the period between each mass measurement was in the order of several days. At

temperatures greater than room temperature, the atmosphere within the desiccator was flushed with nitrogen before sealing to reduce the impact of mass loss due to bagasse oxidation.

2.11. Results and discussion

2.11.1. Saturation moisture contents

Figure 2.11.1 shows moisture sorption histories of bagasse samples that were maintained at the indicated humidity at a temperature of 3°C.

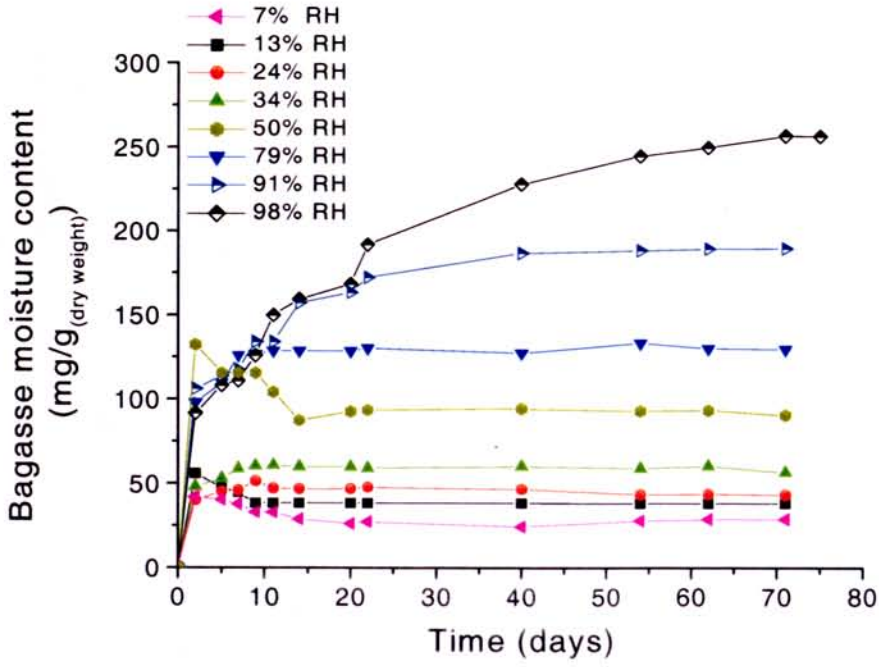

Figure 2.11.1: An example of moisture data for measurements temperature at 3 ℃.

Figure 2.11.1 shows typical moisture sorption data for this study. These data illustrate the rate at which each bagasse sample achieved its equilibrium moisture content at the humidity investigated. Each moisture value shown represents a mean of three separate sub-samples. Notice that during the first twenty days of the measurements, the samples exposed to 7, 13 and 50% humidity displayed different behaviour to the other samples, with the initial moisture concentration temporarily increasing above the final equilibrium value. The origins of this occurrence is not clear and since the data suggests that the final equilibrium moisture value is unaffected by this perturbation, this aspect has not been investigated further. Notice that at high relative humidity, a period in excess of 60 days was

required for the sample to reach constant mass. This aspect was to prove to be a severe disadvantage of this method and limited the range of temperatures that could be realistically examined. Bagasse samples from two seasons were examined, one from the 1996 season and one from the 1998 season. The moisture sorption data for the range of temperatures examined for each season are presented individually in figures 2.11.2 and 2.11.3.

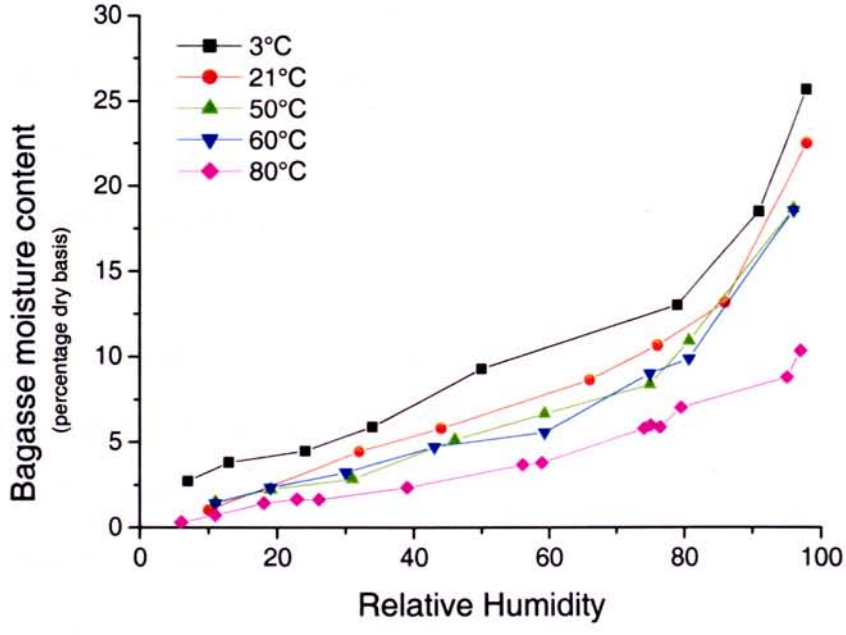

Figure 2.11.2: Combined equilibrium moisture plot for bagasse from the 1998 season.

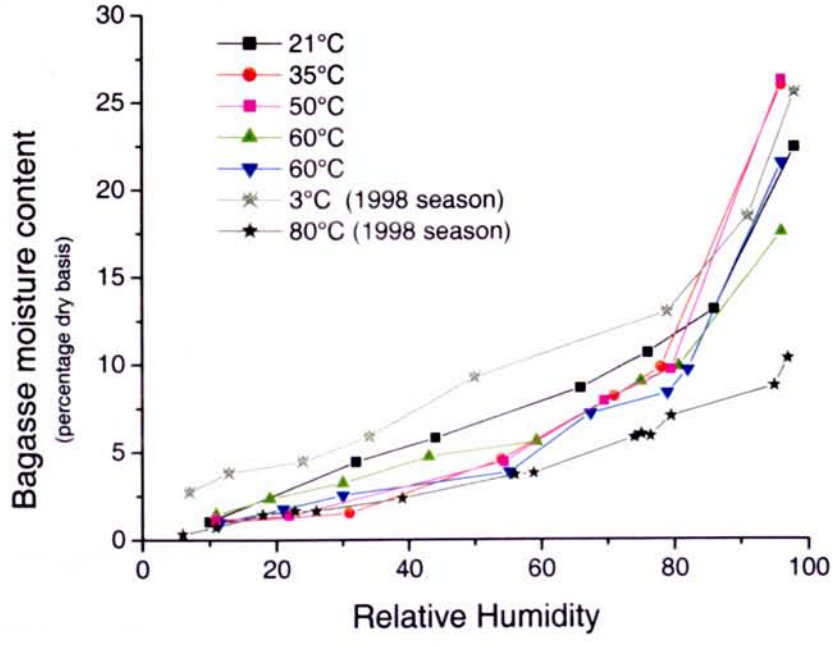

Figure 2.11.3: Combined equilibrium moisture concentration plot for bagasse from the 1996 season.

Both of the above sets of data (figure 2.11.2 and 2.11.3) show similar general trends with respect to moisture and temperature with a nearly exponential increase in moisture at high humidity and an inverse moisture dependence with respect to temperature. These data for bagasse from the 1998 season shows more defined temperature dependence, while these data for the 1996 season shows some overlap between the moisture concentration values at higher temperatures. Generally, however, little difference in moisture content is displayed between these two sets of data for a similar moisture content value. For comparison, the moisture data at 3°C and 80°C from the 1998 season have been included on the figure 2.11.3. Notice that these moisture data from the 1996 season generally falls within the range measured for the 1998 season.

Allardice (1968) has suggested a model for the interpretation of the nature of the moisture sorption of coal that is plausible for bagasse. The Allardice (1968) interpretation suggests that the sigmoid shape displayed by coal indicates that three separate sorption processes are occurring. The first process described by Allardice (1968), which is not clearly shown in the current bagasse moisture data, consists of a monolayer sorption region that occurs at low humidity values. In this region, water hydrogen bonds directly to the hydroxyl groups of the bagasse surface. Allardice (1968) suggests that this region exists below about 10% relative humidity in brown coal. The second region identified by Allardice (1968) is a 'multilayer condensation' region. In these current data, this region is indicated by the nearly straight-line section in the middle of the isotherm. This region consists of water that is weakly hydrogen bound to the water molecules on top of the monolayer. The Allardice (1968) analysis suggests that a third region, identified as the 'capillary condensation' region, is identified by the concave portion of the isotherm. In this region, the water condenses in the capillaries of the bagasse and with further condensation, leads to bulk or 'free' water on the bagasse surface.

Using these current data, the approximate calorimeter/reactor inlet gas stream humidity required to maintain a constant moisture concentration within the bagasse sample was identified. These data suggest that the saturated sorption moisture value for bagasse is of the range of ~25 to 35%. Hence, at bagasse moisture levels above this value a saturated inlet gas streams was utilized.

While not the main objective of this study, it is instructive to calculate the isosteric heat of sorption from these data or the "ΔH for a particular surface coverage" (Atkins 1982 p1024; Allardice, 1968). Following the analysis of Allardice (1968) and using the Clausius-Clapeyron equation in a form defined by:

$$\frac{\partial \ln p}{\partial T_v} = q_{st} / RT^2 \qquad [2.3]$$

where p is the vapour pressure, T is the temperature, R is the universal gas constant, while q_{st} is defined as the isosteric heat of sorption. By integrating equation 2.3 and assuming that the quantity of sorption water vapour remains constant for the duration of the measurement, the isosteric heat can be evaluated for the selected temperature and surface coverage. The isosteric heat values are obtained graphically from the slope of the plot of p against 1/T with p plotted on a logarithmic scale. The above assumption arises due to the condition that isosteric heat is a function of moisture coverage. The corresponding plot is shown in figure 2.11.4.

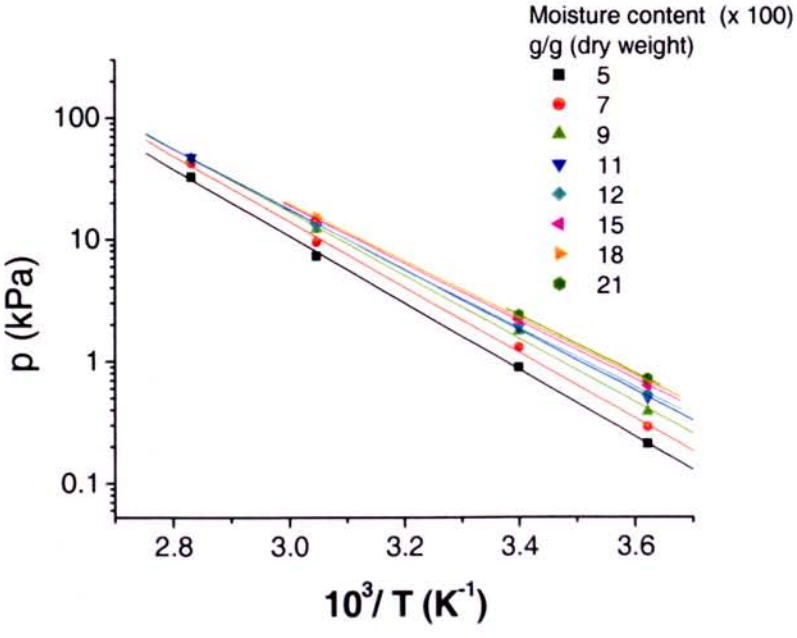

Figure 2.11.4: A plot of p against 1/T at constant bagasse moisture content for a bagasse sample from the 1998 season.

The linearity of the above Clausius-Clapeyron isoteres provides an indication as to the validity of the assumptions of this model and hence, its application to the bagasse system. The linearity of these current data is a feature that is consistent with similar data for brown coal (Allardice, 1968). From the

slope of the Clausius-Clapeyron isoteres (figure 2.11.4.) at each bagasse moisture concentration, the isosteric heat of sorption can be calculated at each bagasse moisture concentration. The isosteric heat of sorption, as a function of moisture content, is shown in figure 2.11.5.

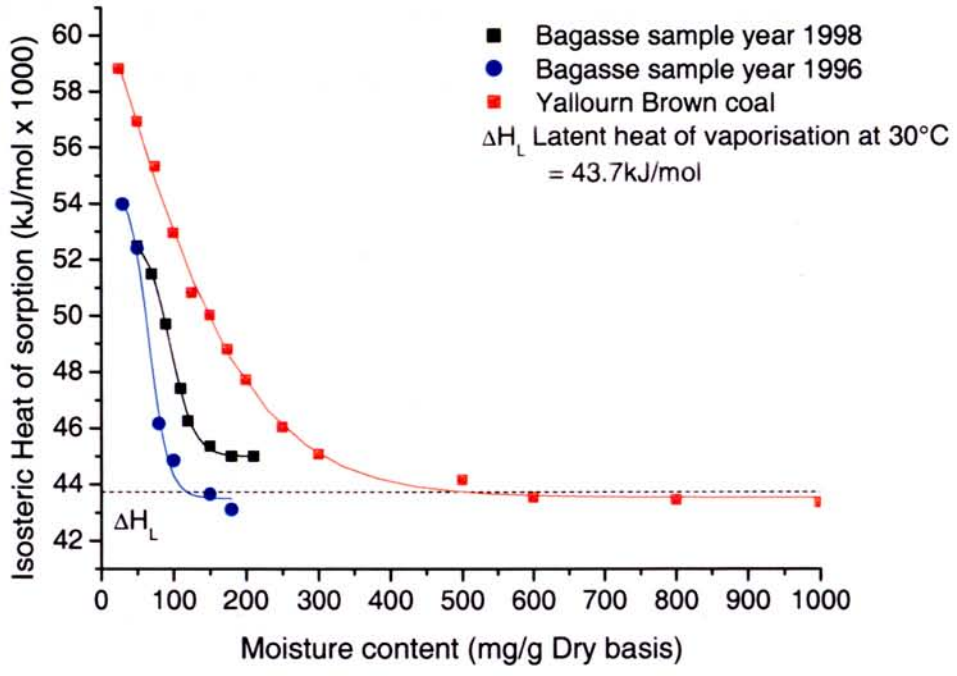

Figure 2.11.5: Clausius-Clapeyron isosteric heat of sorption as a function of moisture content for bagasse samples from the 1996 and 1998 seasons.

These isosteric sorption data for the two bagasse seasons that are displayed in figure 2.9.5 exhibit similar general trends. In both cases the enthalpy increases rapidly to a maximum of 52 kJ/mol for the 1998 season and 54 kJ/mol for the 1996 season as the moisture content falls below ~16% (dry basis) and ~13% (dry basis) for each respective season. These current data show a variation in the isosteric heats between the two seasons and it is unclear if this is a result of seasonal variation or an indicator of the variation and uncertainty of this experimental method.

While clearly more work is required in this area to determine the detailed nature of the water sorption process of bagasse, these current data suggest that the interpretation of Allardice (1968) regarding the nature of the bonding of water for coal is plausible for bagasse. In both the current bagasse and the coal data, the region of maximum isosteric enthalpy is consistent with reported hydrogen bonding energies (Allardice, 1968). The region of rapidly decreasing isosteric enthalpy suggests that the bond

strength quickly reduces as multiple water layers develop. At moisture concentrations of approximately 150 to 300 mg/g, capillarity condensation and then free water develops.

While this sorption study possesses a number of experimental shortcomings compared to the in-depth sorption study on Yallourn coal by Allardice (1968), these data have elucidated important aspects regarding the nature of moisture sorption of bagasse.

2.11.2. Oxidation rates

Figure 2.11.6. shows the oxidation rate as a function of time at a temperature of 70°C and at a moisture content of 100% (dry basis) for bagasse from the 1997 season-batch 1.

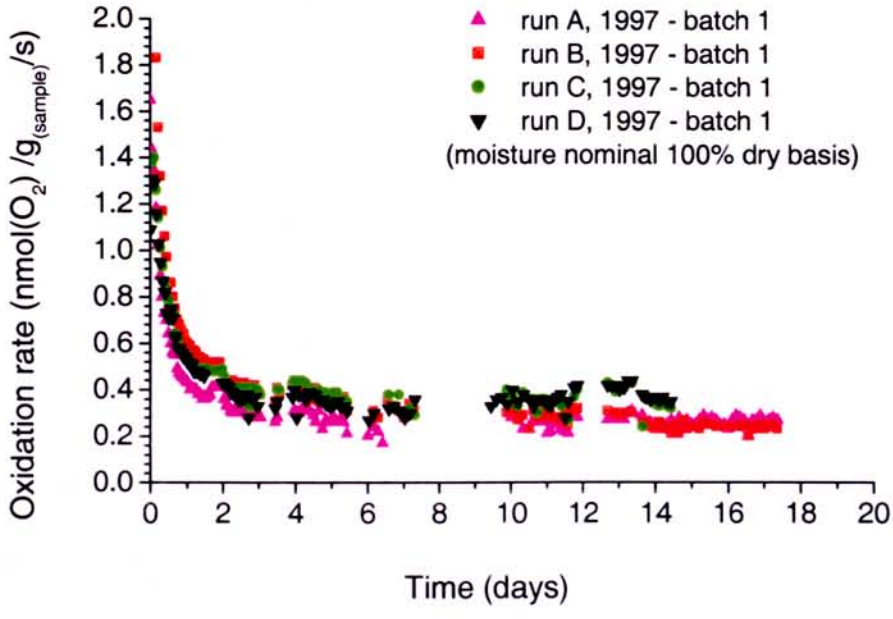

Figure 2.11.6.: Time dependence of bagasse oxidation rate at 70 °C.

Four individual runs were carried out and these data show the reproducibility of the results. For these data, the oxidation rate decreased uniformly from a maximum at the beginning of the run to a steady state value after ~ 6 days. These data illustrate the time dependence of the rate of bagasse oxidation and display an steady state oxidation rate of 0.35 ±0.1 nmol(O_2)/$g_{(sample)}$/s. Uncertainty quoted

represent bounds of the scatter of the experimental data over the steady state region. This type of oxidation behaviour was found to be characteristic of this sample for the temperatures investigated.

Figure 2.11.7.: shows the oxidation rate as a function time, again for bagasse from the 1997 season-batch 1 but at a temperature of 50°C.

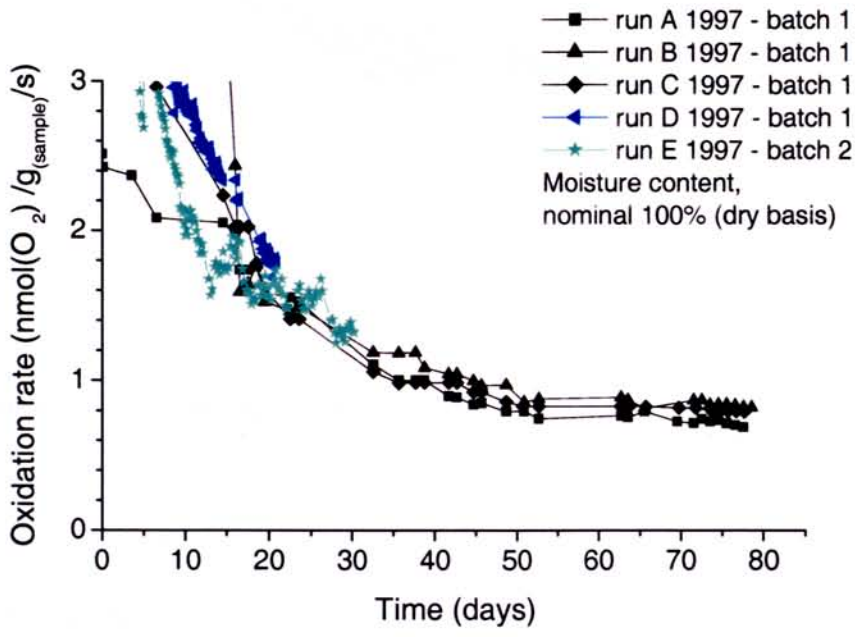

Figure 2.11.7.: Time dependence of bagasse oxidation rate at 50 °C

Figure 2.11.7.: shows data from five oxidation measurements at 50°C. In this figure, runs A, B and C suggest that an apparent steady state has been reached by the sample after approximately 50 days. Runs D and E were terminated prematurely but have been included for completeness. Notice that runs D and E display the general initial trends common to runs A, B and C. These current data also display different time behaviour to the data shown in figure 2.9.6 with the current data requiring in excess of 55 days for the oxidation rate to decline from a local maximum to a constant value. The origin of the variable time dependent behaviour is an aspect that has continued to remain unclear throughout this study. For these current data, a constant oxidation rate of 0.85 ±0.1 nmol(O_2)/$g_{(sample)}$/s was displayed after approximately 60-70 days..

Figure 2.11.8 shows similar data to Figure 2.11.7, but this time at a temperature of 35°C.

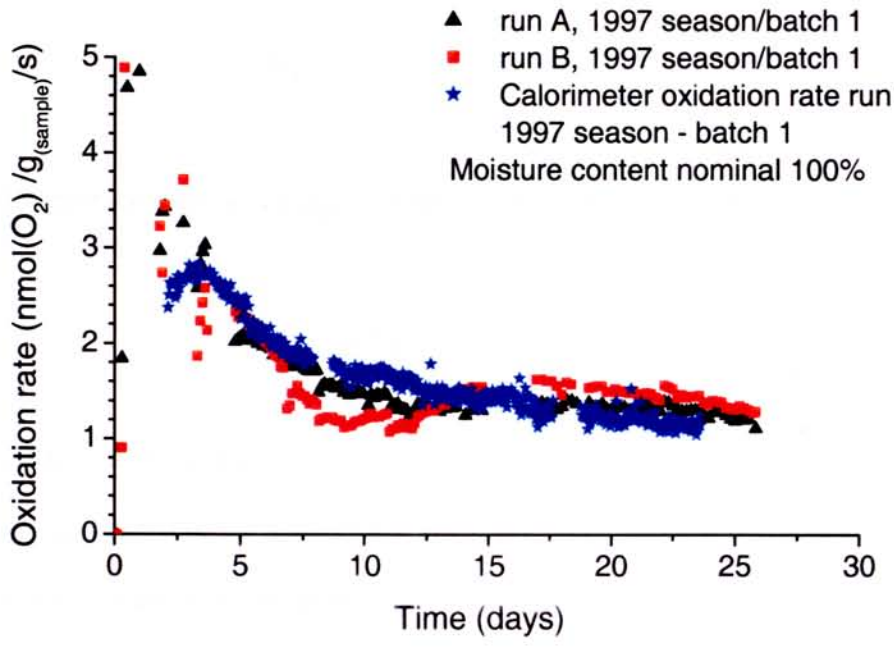

Figure 2.11.8.: Time dependence of bagasse oxidation rate at 35 ℃.

Figure 2.11.8.: shows general features that were displayed in Figure 2.11.7 with the oxidation rate again relaxing from an initially large value to a smaller value. These current data, however, show a number of important differences. Notice that after 10 days the oxidation rate of both runs A and B increase to local maxima after approximately 6 days then reduces and approaches the oxidation rate of day 10. This type of feature has also been observed in similar oxidation measurements of coal (Carras, 2000). The other important feature relates to the peak that occurred within the first 5 days of the three runs displayed in this figure. This was a commonly observed phenomenon in the bagasse data and while the precise nature of the reactions are at present unknown, this phenomenon has been observed previously in general kinetics studies. It may be shown that this phenomenology can be modelled as a consecutive pair of first order chemical reactions as shown below (Atkins, 1982).

If: $$A \xrightarrow{k_1} B \xrightarrow{k_2} C$$

$$\frac{d[B]}{dt} = k_1[A] - k_2[B]$$

$$[A]_t = [A_0]e^{-k_1 t} \qquad [2.4]$$

If for B the condition $[B]_0 = 0$ is assigned the above integrates to:

$$[B]_t = [A]_0 \frac{k_1(e^{-k_1 t} - e^{-k_2 t})}{k_2 - k_1} \qquad [2.5]$$

By differentiating and assigning d[B]/dt = 0, th e time at which this occurs is:

$$t_{max} = \frac{\ln(k_2/k_1)}{k_2 - k_1} \qquad [2.6]$$

with $[B]_{(0)} = 0$, $[B]_{(\infty)} = 0$.

The concentration of the intermediate B will rise from zero to a maximum, and then return to zero as the initial reactant A is consumed. The magnitude of the intermediate concentration will be, therefore, determined by the ratio of the reaction constants k_1 and k_2. There are a lot of simple schemes, such as chain reactions involving free radicals, which will give a maximum at some intermediate time.

It should be noted that the results of the oxidation measurements shown in figures 2.11.6, 2.11.7 and 2.11.8 display very unusual heating behaviour. The oxidation rate measurements for bagasse from the 1997 season displayed behaviour where the oxidation rate tended to increase with decreasing temperature. This was unexpected and it is unclear as to the origin if this behaviour. It is suspected that it may be a seasonal characteristic as it was not displayed in results from the other two seasons examined. It should be noted that most of the measurements discussed in this chapter were completed using bagasse from the 1997 season with a very limited number of measurements undertaken on bagasse from the 1998 season. Hence, the interpretation and comparison of these results is most difficult.

2.11.3 Moisture dependence

Figure 2.11.9. shows the rate of oxidation as a function of time and moisture content for a second bagasse batch from the 1997 season. The measurement was completed at a temperature of 60°C.

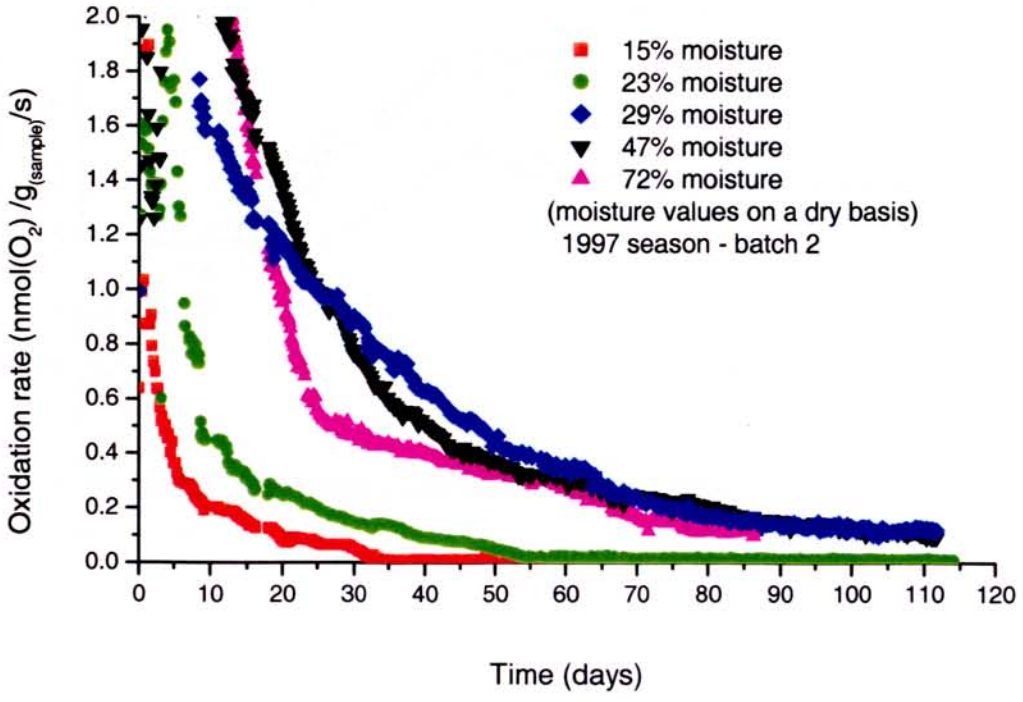

Figure 2.11.9: Moisture dependence of bagasse oxidation rate at 60 °C.

Data shown in figure 2.11.9 display a clear dependence with respect to moisture content, with the rate of oxidation decreasing to negligible levels for moisture contents between 23 and 29%. Correspondingly, at moisture contents above this range, significantly greater oxidation rates of between 0.9 and 0.5 $nmol^{-1}/g/s$ were measured. This similar behaviour was observed by Bainbridge and Carras (1995) with small rates of oxidation being measured at low moisture values.

A similar behaviour to that shown in figure 2.11.9, was also observed at 90°C. The moisture dependence of the oxidation rate at 90°C is shown in figure 2.11.10:

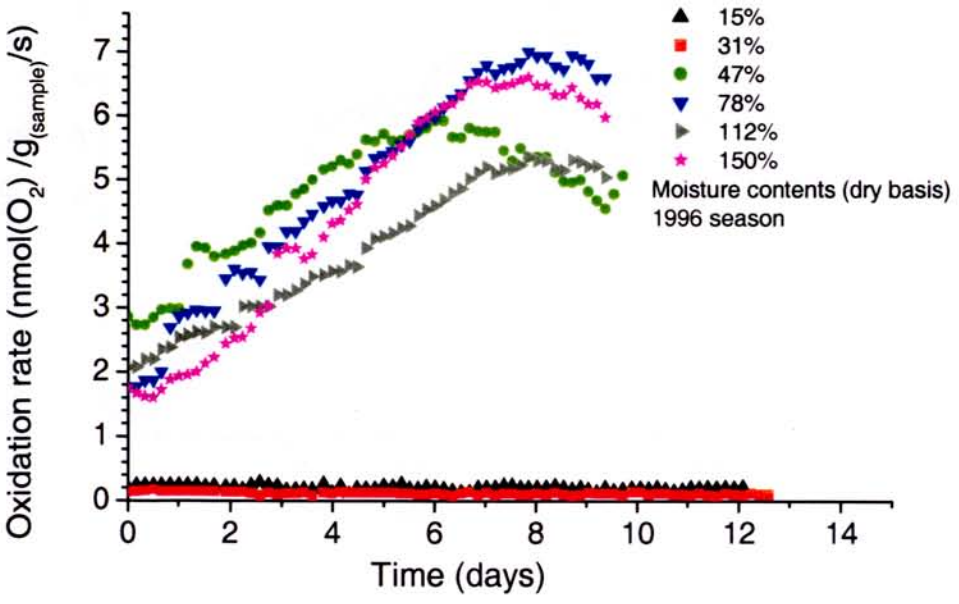

Figure 2.11.10: Moisture dependence of bagasse oxidation rate at 90℃.

Data shown in the above figure displays similar moisture dependent behaviour to those displayed in figure 2.11.9. At bagasse moisture values less than about 30%, the bagasse samples display negligible reactivity while at moisture content greater than 30%, the rate of oxidation increases until limited by reactant consumption. After day 12, the four samples with moisture contents above 35%, exhibited significant darkening of the bagasse fibre and an odour that was characteristic of the high temperature decomposition within commercial bagasse stockpiles. Conversely, little visual change and little odour was displayed by the lower moisture content samples. Notice that these current data also exhibit a different time dependent behaviour to the previously examined data.

Figure 2.11.11 displays the time dependent oxidation behaviour for bagasse from the 1998 season and at a temperature of 75°C.

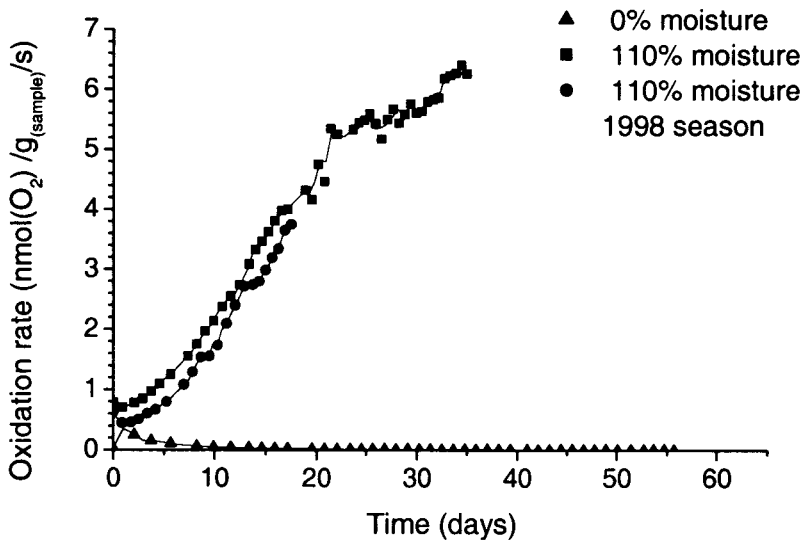

Figure 2.11.11: Moisture dependence of bagasse oxidation rate at 75℃.

Data displayed in Figures 2.11.9, 2.11.10. and 2.11.11. shows clearly the existence of two well defined reaction regimes that are strongly moisture dependent. These data suggest the existence of a 'dry' reaction and a 'wet' reaction with the wet reaction significantly more reactive at low temperatures. These data, in combination with the moisture data from section 2.10.1 suggest that the onset of the wet reaction occurs when bagasse moisture contents increases to concentration range where unbound water exists within the bagasse sample. Notice also the different time dependent behaviour exhibited by this sample which is consistent with data from the 1996 season.

Figure 2.11.12.: shows the oxidation rate of the 60°C data displayed in figure 2.11.9: at 100 days. In this current figure these data are displayed as a function of moisture content.

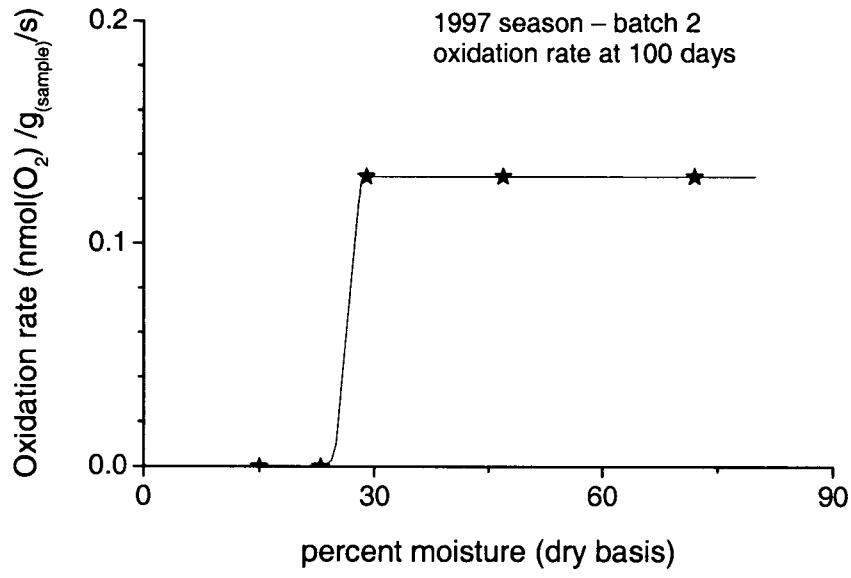

Figure 2.11.12: Moisture dependence of bagasse oxidation rate at 60℃. Oxidation rates shown are steady state values at 100 days.

Note the step change at a moisture content of ~21% indicating the onset of the wet reactions. Figure 2.11.13 shows a similar plot for data from Figure 2.11.10 for the bagasse at a temperature of 90°C. In this case the data displayed are peak oxidation values

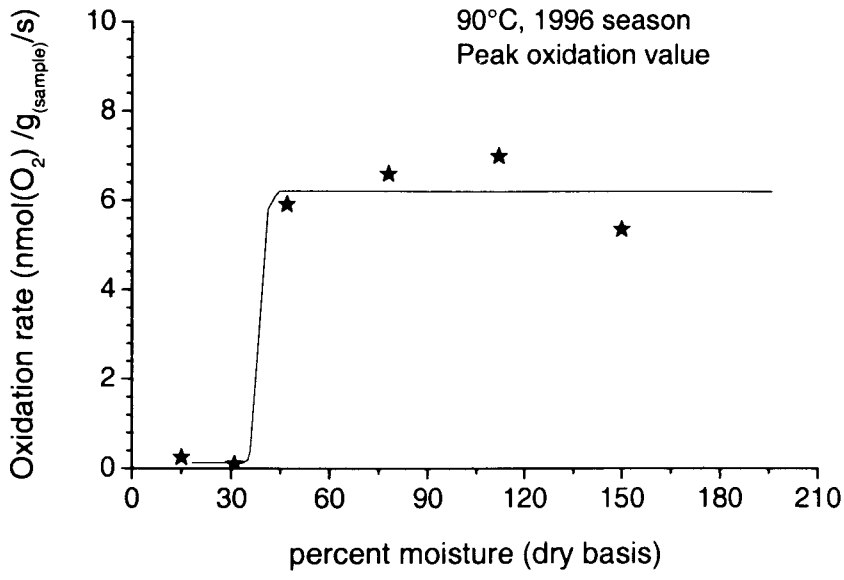

Figure 2.11.13: Moisture dependence of bagasse oxidation rate at 90℃. Oxidation rates shown a peak oxidation rates.

While the trend in these data is similar to that shown in Figure 2.11.12 (with a step change at similar moisture content), the oxidation rates at the higher temperatures are correspondingly larger.

2.11.4. Seasonal differences

The results shown in section 2.11. were from two seasons, 1997 and 1998. A comparison of the oxidation data for the three seasons examined are shown in figure 2.11.14.

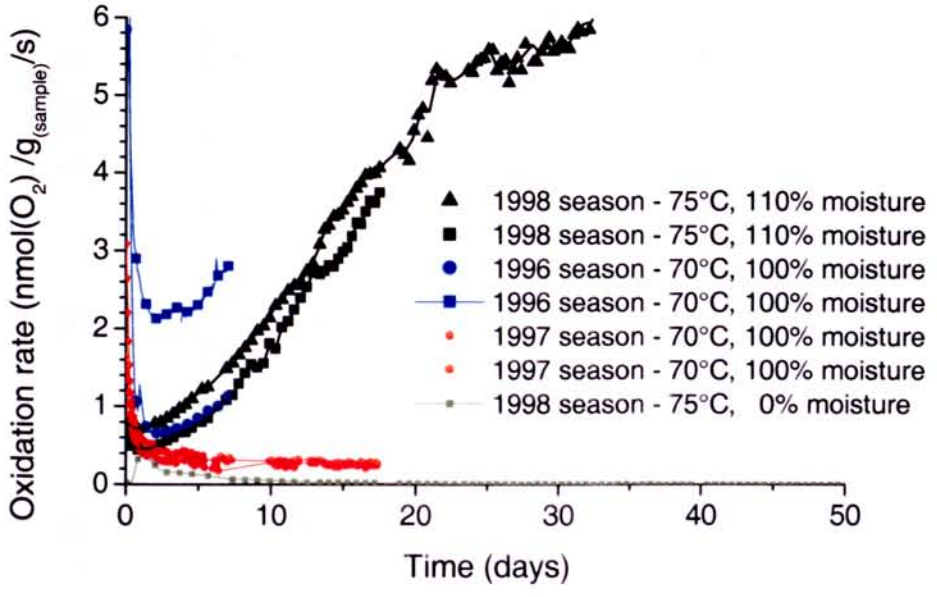

Figure 2.11.14: Seasonal differences of bagasse oxidation rates.

These data presented in figure 2.11.14: suggest two types of behaviour for the three samples examined. Notice that these oxidation data for the three bagasse samples display similar behaviour for the first 1 to 2 days, however, after this time, the oxidation rates of the samples from the 1996 and 1998 increase for in excess of 30 days for the 1998 season samples. These two seasons are in contrast to the oxidation rate behaviour of samples from the 1997 season, which approach a steady state oxidation rate after 10 days.

2.11.5. Effect of temperature

Results of bagasse oxidation measurements presented in this chapter are displayed in table 2.3.

Table 2.3 Combined Oxidation Rates for each bagasse season.

	Oxidation rate of each sample type. (nmol/g/s)		
Temperature (°C)	1996	1997 – batch 1	1997 – batch 2
35		0.23	
		0.4	
		0.06	
50		0.95	
		0.91	
		0.77	
55			0.5
58		0.56	
60	0.29		0.09
	0.4		0.15
	0.8		0.16
70	3.1	0.28	
	3.0	0.31	
		0.42	
		0.42	
90	6.6		
	6.3		
	6.9		
	5.8		

Results presented in sections 2.11.2 to 2.11.4 are summarized in the above table. These data clearly show that the bagasse oxidation chemistry is complex. The variability of the results combined with the limited data do not enable direct conclusions to be drawn regarding the general, temperature dependent, oxidation behaviour of bagasse. These data, however, reveal a number of features specific to the bagasse samples studied. Firstly, these data reveal the existence of two different types of

oxidation behaviour over the 60 to 70°C temperature range. When oxidation rates for the 1996 season are compared to those of the 1997 season, then a 10-fold increase in oxidation rates are observed. At temperatures of 60°, the difference between the oxidation rates for these two seasons falls to a factor of between 2.5 and 5. If each season is considered individually, then the rapid increase in oxidation rate with respect to temperature for the 1996 season, suggests the existence of a strong Arrhenius type temperature dependence with respect to oxidation rate. The 1997 season, however, suggests a more complex behaviour with a local maximum occurring at 50°C and local minimum at 60 to 70°C. This is clearly an unusual type of behaviour, but one that has been observed in cool flames (Mulcahy, 1973). If these data are considered collectively, then the results suggest oxidation rates of between 0.15 and 0.8 nmol/g/s, which are within oxidation rate range measured at 50°C with bagasse samples from the 1997 season. These data clearly show that significantly more research is required before direct conclusions can be made regarding the general oxidation behaviour of bagasse.

2.11.6. Rate of heat production

Figure 2.11.15 shows oxidation rates of bagasse as measured by the isothermal calorimeter at two temperatures of 35°C and 50°C while figure 2.11.15 displays the thermal power.

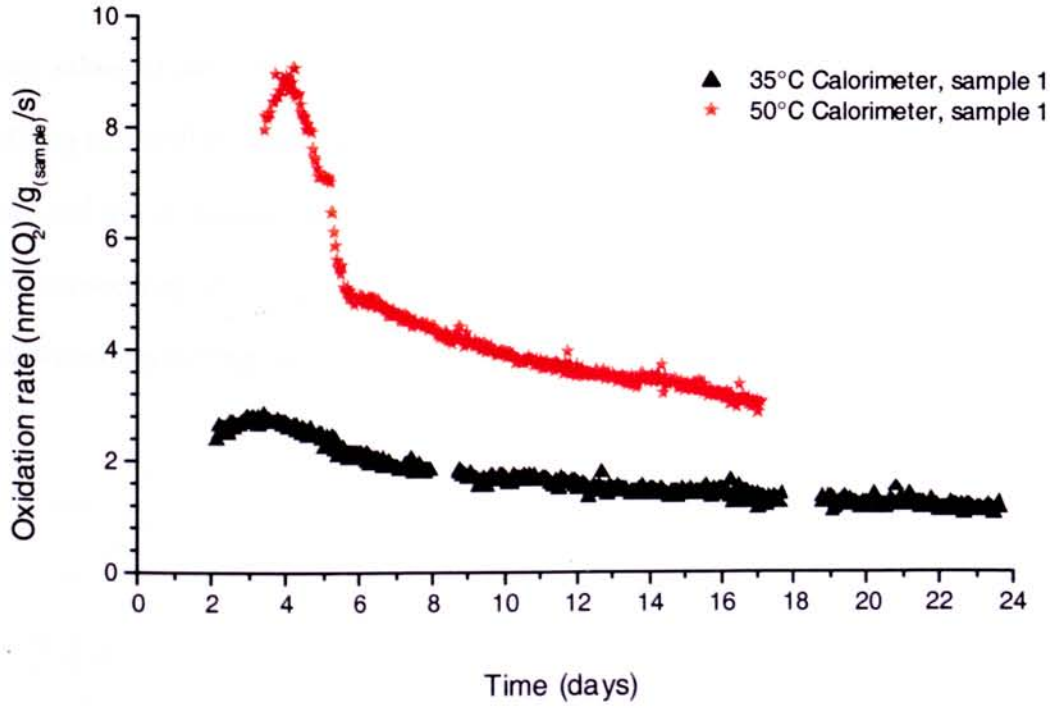

Figure 2.11.15:Time dependence of bagasse oxidation rate at 35 °C and 50 °C.

Figure 2.11.16.: shows the corresponding thermal powers.

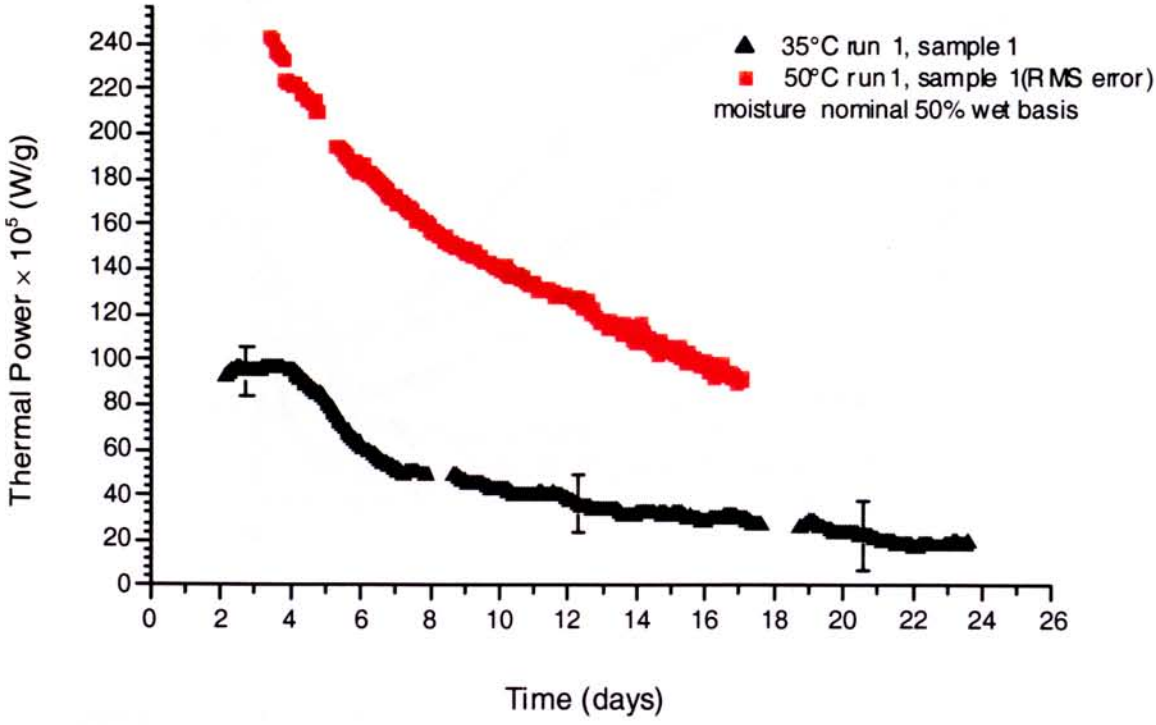

Figure 2.11.16.: Thermal power at 35 and 50 °C.

These values of thermal power are initially large at ~ 2.4mWg^{-1} initially for the sample at 50°C declining to ~1mW g^{-1} after ~14 days. At 35°C the two rates are ~1mWg^{-1} and 0.4mWg^{-1} respectively. These two sets of measurements were for the bagasse sample taken during the 1997 season and if the initial transient up until day 6 of the 50°C data is excluded, these data suggest that the rate of heat generation from the bagasse is directly related to the rate of oxygen consumption.

Figure 2.11.17. shows similar data but this time for the bagasse sample from the 1996 season.

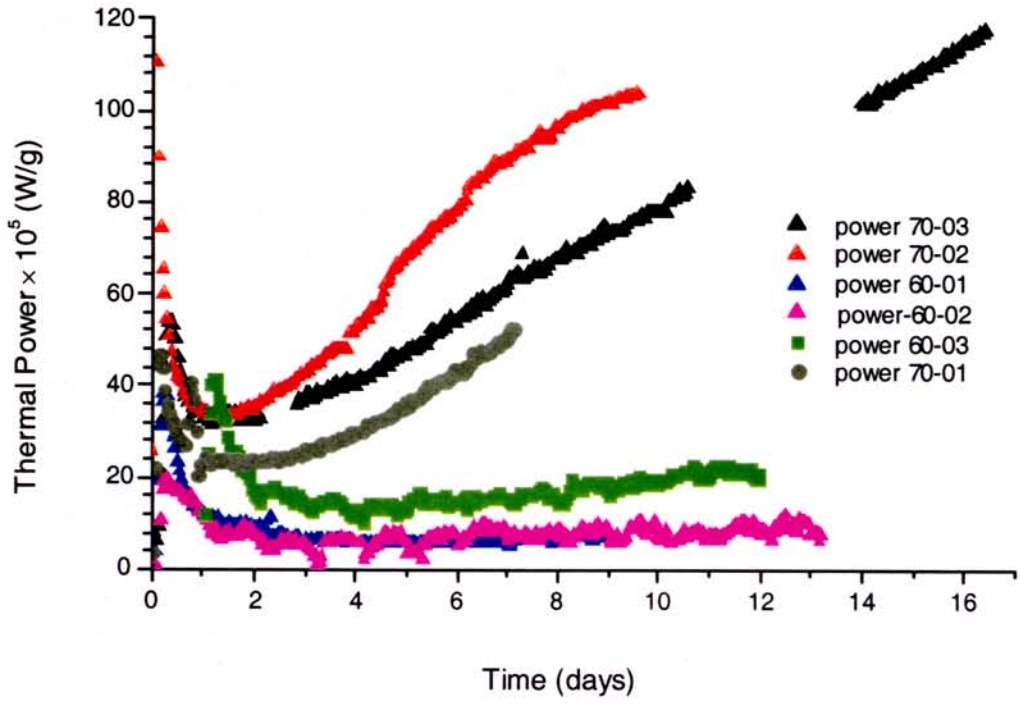

Figure 2.11.17: Thermal power at 60 and 70 °C.

Notice the different behaviour displayed by these data shown in Figure 2.11.17. to data shown in Figure 2.11.16. The bagasse in this current case, exhibits thermal behaviour similar to the oxidation behaviour displayed in Figures 2.11.10. and 2.11.11. While the oxidation rates in Figures 2.11.10. and 2.11.11 increase and reach a peak after 8 days in Figure 2.11.10. and 30 days in Figures 2.11.11. the initial trend of a accelerating kinetics is clearly displayed. These data in Figure 2.11.17 show that the peak was still being approached when the runs were inadvertently terminated after a time period of 10 days.

The relationship between the rate at which heat is released from a reaction and the rate at which oxygen is consumed is an important thermodynamic quantity. The ratio of heat release per mol of oxygen over the duration of the calorimeter measurements at 35, 50, 60, 70 and 90°C is displayed in figure 2.11.18.

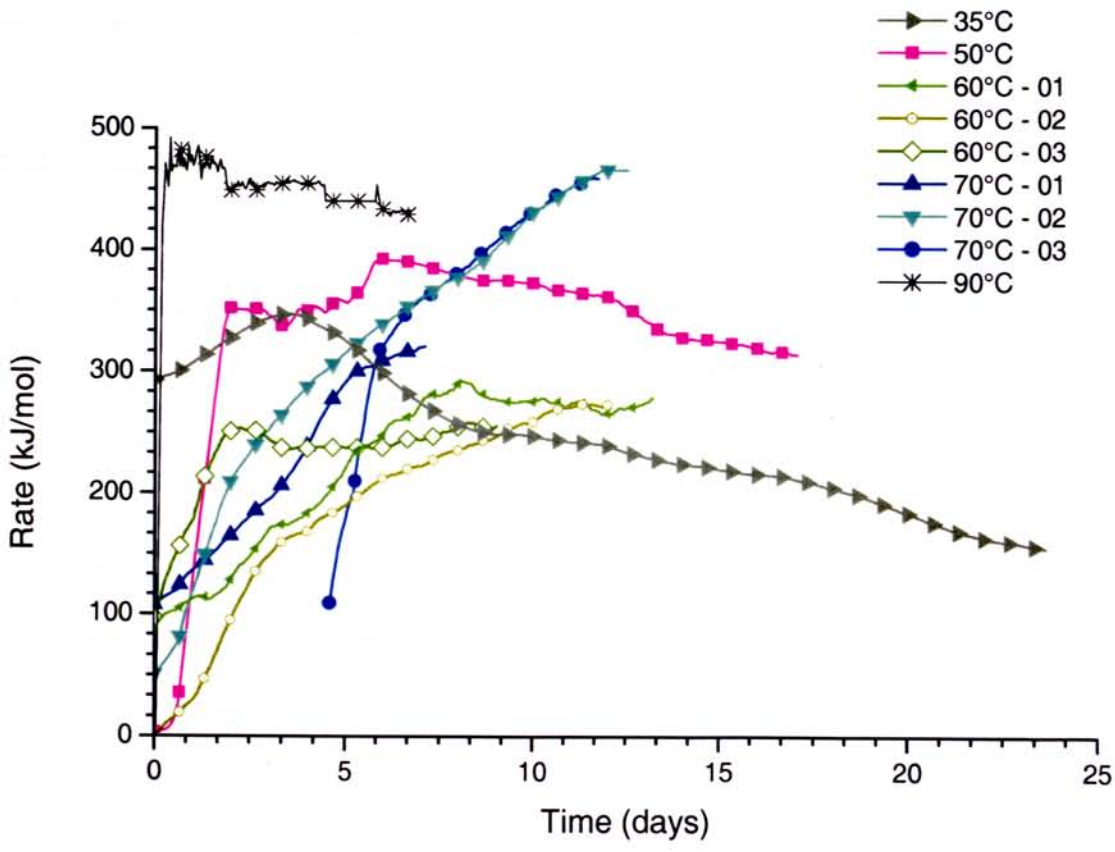

Figure 2.11.18.: Ratio of heat release per mole of oxygen (kJ/mol(O_2)) at 35, 50, 60, 70 and 90 °C.

These data displayed in figure 2.11.18 suggest that the ratio of the heat released per mol of oxygen is in the range between 150 to 490 kJ/mole O_2 over the temperature range studied. These heat release rate data are in the range measured by other researchers; 207 kJ/mol (O_2) for groundnut oil/sawdust mixture (Bowes, 1984; page 267), 222 to 343 kJ/mol (O_2) for the oxidation of palm kernel oil (Bowes, 1984; 268), and between 250 and 380 kJ/mol (O_2) for coal (Carras and Young, 1994). The latter coal measurements were completed using isothermal calorimetry methods with most values in the range 300 – 380 kJ/mol (O_2).

These results presented above highlight the complex nature of the self-heating chemistry of bagasse and the difficulty of obtaining comprehensive heat release data for this material. Experiments have required long continuous measurement periods. Inevitably, the long time periods required to complete

this current study have resulted in a number of premature terminations of experiments which were a result of both equipment failure and the inadvertent termination of the experiment before completion.

2.12 Conclusions

The current experimental study is the first attempt to investigate the self-heating oxidation and heat release chemistry of bagasse. The present experimental study has revealed three key properties of bagasse undergoing oxidation in the presence of atmospheric oxygen.

a) Bagasse exhibits strong moisture dependence with respect to reaction rate at moistures greater than 30% (dry basis). Negligible reaction is displayed at moisture contents below 25 to 30%, while at moistures above this value, oxygen consumption rates of up to 6 $nmolg^{-1}s^{-1}$ are displayed.

b) At temperatures of 50°C oxidation rates in the order of 0.8 nmol/g/s (O_2) have been measured while at 60°C oxidation rates between 0.09 and 0.8 nmol/g/s. (O_2) Peak oxidation rates of 3.1 nmol/g/s and 6.9 nmol/g/s (O_2) have been measured at 70°C and 90°C respectively.

c) The rate of heat generation from bagasse has been measured to in the range from between 150 and 490 kJ/mole O_2, over the temperature range from 35 to 90°C.

d) The oxidation chemistry of bagasse is complex with samples from different seasons displaying significantly different oxidation and heating behaviour. Bagasse from the 1997 season displayed reduced reactivity compared to the sample from the 1996. It is not known whether this difference is due to seasonal or regional factors as the exact source of the bagasse is unknown. This, however, requires further investigation.